UNIVERSITY OF HELSINKI

Evaluation of a CRISPR-Cas9-based strategy for modeling keratitis fugax hereditaria in THP-1 cells

Master’s programme in Translational Medicine
Study track: Health Industry and Innovations
Master's thesis

Author:
Julia Koskela

Supervisors:
Docent MD PhD Joni Turunen
PhD researcher Sabita Kawan

7.10.2026
Helsinki

Faculty: Faculty of Medicine
Degree programme: Translational Medicine
Study track: Health Industry and Innovations
Author: Julia Koskela
Title: Evaluation of a CRISPR-Cas9-based strategy for modeling keratitis fugax hereditaria in THP-1 cells
Level: Master's degree
Month and year: 10/2026
Number of pages: 64
Keywords: keratitis fugax hereditaria, NLRP3, CRISPR-Cas9, disease modeling, inflammasome, THP-1 cells, homology-directed repair, gene editing
Supervisor or supervisors: Joni Turunen, Sabita Kawan
Where deposited: E-Thesis, Helda
Abstract:

Keratitis fugax hereditaria (KFH) is an autosomal dominant corneal disease caused by the pathogenic c.61G>C, p.(Asp21His) variant in the *NLRP3* gene. KFH is characterized by recurrent episodes of ocular pain, photophobia, and corneal inflammation, which may lead to permanent stromal opacities and visual impairment. The variant is associated with increased NLRP3 inflammasome activity, resulting in enhanced secretion of the pro-inflammatory cytokine interleukin-1β (IL-1β). Although the genetic cause of KFH has been identified, the cellular mechanisms underlying disease pathogenesis remain elusive. The development of a functional *in vitro* disease model would provide a platform to study the disease mechanisms and support potential development of targeted therapeutic approaches in the future.

The aim of this thesis was to generate an *in vitro* model of KFH by introducing the *NLRP3* c.61G>C variant into the human monocytic THP-1 cell line using CRISPR-Cas9 gene editing. A cryopyrin-associated periodic syndrome (CAPS)-associated *NLRP3* c.778_780delinsTGG, p.(Arg260Trp) variant was included as a positive control. Edited cells were sorted with fluorescence-activated cell sorting (FACS), expanded as single-cell clones, and screened using polymerase chain reaction (PCR), restriction digestion, and Sanger sequencing.

FACS analysis demonstrated efficient delivery of CRISPR-Cas9 components into THP-1 cells, as the edited cell populations were successfully enriched with a

fluorescence marker. However, only a limited number of single-cell clones expanded after sorting. Molecular analyses did not confirm introduction of either the KFH-associated variant or the CAPS-associated control variant in the analyzed clones. One KFH-targeted clone showed an atypical restriction digestion pattern and ambiguous sequencing results, suggesting a possible alteration at the target locus, although successful editing could not be confirmed.

In conclusion, a validated KFH disease model was not obtained under the conditions tested. Although flow cytometry indicated uptake of fluorescently labeled tracrRNA, the intended *NLRP3* variants were not confirmed in the small number of clones examined. Limited clonal recovery and unresolved genotyping results prevented firm conclusions about editing efficiency and the factors limiting model generation. Further work should prioritize verification of guide and donor designs, assessment of editing in bulk cell populations, and optimization of clonal recovery to support the development of a validated model for investigating KFH-associated NLRP3 inflammasome activity.

Table of contents

Abbreviations *6*

1 Introduction *8*

1.1 Innate immunity **8**

1.2 NLRP3 inflammasome **9**

1.2.1 Structure and function 10

1.2.2 Activation mechanism 11

1.3 NLRP3 gain-of-function diseases **12**

1.3.1 Cryopyrin-associated periodic syndromes 12

1.3.2 NLRP3 in CAPS 13

1.4 Cornea and ocular immune regulation **14**

1.4.1 Corneal anatomy 14

1.4.2 Ocular immune privilege 15

1.5 Keratitis fugax hereditaria **16**

1.5.1 Clinical characteristics and epidemiology 16

1.5.2 Genetic background and diagnosis 16

1.5.3 Current understanding of disease mechanisms 17

1.6 Functional disease modeling **18**

1.6.1 THP-1 cells 18

1.6.2 CRISPR-Cas9 gene editing 19

2 Aim of the thesis *22*

3 Materials and Methods *23*

3.1 Cell culture **23**

3.2 Experimental design **23**

3.3 CRISPR-Cas9 ..... **25**

3.3.1 CRISPR-Cas9 target and donor design 25

3.3.2 CRISPR reagents 26

3.3.3 gRNA annealing and RNP complex formation 27

3.4 Electroporation **27**

3.4.1 Preparing cells for electroporation 27

3.4.2 Electroporation procedure 28

3.5 Fluorescence-Activated Cell Sorting (FACS) 28
3.5.1 Sample preparation and initial sorting 29
3.5.2 Single-cell sorting 29
3.6 Screening of cultured clones 30
3.6.1 DNA extraction 30
3.6.2 Amplification of DNA 30
3.6.3 Restriction digestion 31
3.6.4 Sanger sequencing 32
4 Results 35
4.1 Nature of THP-1 cell growth and maintenance 35
4.2 Fluorescence-Activated Cell Sorting 36
4.3 Assessing the CRISPR edit in THP1 cells 43
4.4 Validation of the edit with Sanger sequencing 45
5 Discussion 49
5.1 Evaluation of CRISPR-Cas9 delivery strategy 49
5.2 Factors potentially limiting the gene editing 49
5.3 Survival of sorted cells 51
5.4 Future aspects 53
5.5 Conclusions 54
6 Acknowledgments 55
References 57
Use of AI 64

Abbreviations

AIM2	Absent in Melanoma 2
ASC	Apoptosis-associated speck-like protein containing a CARD
ATP	Adenosine triphosphate
CAPS	Cryopyrin-associated periodic syndromes
CARD	Caspase activation and recruitment domain
Cas9	CRISPR-associated protein 9
cGAS	Cyclic GMP-AMP synthase
CINCA	Chronic infantile neurologic cutaneous articular syndrome
CLR	C-type lectin receptor
CO_2	Carbon dioxide
CRISPR	Clustered regularly interspaced short palindromic repeats
crRNA	CRISPR RNA
DAMP	Damage-associated molecular pattern
DMSO	Dimethyl Sulfoxide
DNA	Deoxyribonucleic acid
DSB	Double-strand break
ECM	Extracellular matrix
FBS	Fetal bovine serum
FACS	Fluorescence-activated cell sorting
FCAS	Familial cold autoinflammatory syndrome
FSC	Forward scatter
gRNA	Guide RNA
GSDMD	Gasdermin D
HDR	Homology-directed repair
IL	Interleukin
IRF	Interferon regulatory factor
KFH	Keratitis fugax hereditaria
LPS	Lipopolysaccharide
LRR	Leucine-rich repeat
MAPK	Mitogen-activated protein kinase
MIM	Mendelian inheritance in man
mtDNA	Mitochondrial DNA

MWS	Muckle-Wells syndrome
NACHT	NAIP, CIITA, HET-E and TP1
NEK7	NIMA-related kinase 7
NF-κB	Nuclear factor kappa B
NHEJ	Non-homologous end joining
NLR	NOD-like receptor
NLRP3	NLR family pyrin domain containing 3
NOMID	Neonatal-onset multisystem inflammatory disease
PAM	Protospacer adjacent motif
PAMP	Pathogen-associated molecular pattern
PBS	Phosphate-buffered saline
PBMC	Peripheral blood mononuclear cell
PCR	Polymerase chain reaction
PMA	Phorbol 12-myristate 13-acetate
PRR	Pattern recognition receptor
PYD	Pyrin domain
RLR	RIG-I-like receptor
RNA	Ribonucleic acid
RNP	Ribonucleoprotein
ROS	Reactive oxygen species
RPMI	Roswell Park Memorial Institute
sgRNA	Single-guide RNA
SSC	Side scatter
ssODN	Single-stranded oligodeoxynucleotide
STING	Stimulator of interferon genes
TIR	Toll/interleukin-1 receptor
TLR	Toll-like receptor
tracrRNA	Trans-activating CRISPR RNA
WT	Wild type

1 Introduction

1.1 Innate immunity

Inflammation is a complex process induced by microbial, viral, or fungal infections, tissue damage, or even autoimmune reactions. The main function of inflammation is to return to a state of homeostasis by resolving the infection or repairing the damage (Barton, 2008; Meizlish et al., 2021; Newton & Dixit, 2012; Soares et al., 2023). Although inflammatory responses differ according to the nature, intensity, and anatomical location of the insult, they share a common logic in which danger signals are sensed, intracellular signaling pathways are activated, inflammatory mediators are produced, and leukocytes are recruited to the affected tissue (Chen et al., 2018; Soliman & Barreda, 2022). This early response is essential not only for antimicrobial defense but also for the initiation of downstream reparative processes, and its magnitude must be tightly controlled because excessive or unresolved inflammation drives tissue injury and inflammatory disease (Soliman & Barreda, 2022; Sundaram et al., 2024).

The immune system is divided into innate and adaptive immune systems (Sáez et al., 2023; Wang et al., 2024). The innate immune system provides the first line of defense and responds rapidly and broadly to pathogens, tissue damage, and homeostatic perturbations through germline-encoded sensing systems (Kawasaki & Kawai, 2014; Sáez et al., 2023). Major innate effector cells include neutrophils, monocytes, macrophages, dendritic cells, and mast cells, while epithelial and endothelial cells can also participate in innate sensing and inflammatory signaling (Chen et al., 2018; Sáez et al., 2023). In contrast, the adaptive immune system depends on antigen-specific receptors on T and B lymphocytes and generates immunological memory, enabling faster and more effective responses upon repeated antigen exposure (Warrick et al., 2025). These two systems are functionally interdependent, because innate sensing instructs antigen presentation, cytokine production, and dendritic-cell activation that shape adaptive immune responses (Kawasaki & Kawai, 2014). In this thesis, we want to focus on the innate immune system.

A central feature of innate immunity is the detection of danger signals by pattern-recognition receptors (PRRs), which are germline-encoded receptors expressed on

cell membranes, within endosomes, in the cytosol, and in some cases in the nucleus (Medzhitov, 2007; Sundaram et al., 2024). PRRs recognize two major classes of signals: pathogen-associated molecular patterns (PAMPs) and damage-associated molecular patterns (DAMPs) (Amarante-Mendes et al., 2018; Chen et al., 2018). PAMPs are conserved microbial structures that are not present in host cells, such as bacterial lipopolysaccharides (LPSs), flagellin, and viral nucleic acids. In contrast, DAMPs are endogenous molecules released from stressed, damaged, or dying cells, for example, ATP and uric acid crystals (Chen et al., 2018; Sundaram et al., 2024; Zindel & Kubes, 2020). Recognition of these signals activates downstream pathways such as NF-κB (nuclear factor kappa B), MAPK (mitogen-activated protein kinase), IRF (interferon regulatory factor), and inflammasome signaling, leading to the expression of cytokines, chemokines, adhesion molecules, type I interferons, and other mediators that coordinate inflammation and host defense (Duan et al., 2022; Kawasaki & Kawai, 2014).

Several PRR families contribute to innate immune surveillance, including NOD-like receptors (NLRs), Toll-like receptors (TLRs), RIG-I-like receptors (RLRs), C-type lectin receptors (CLRs), and AIM2-like receptors (Amarante-Mendes et al., 2018; Duan et al., 2022). Among these, NLRs are particularly relevant to this study. NLRs are cytosolic PRRs that detect intracellular pathogens, sterile danger signals, and cellular stress, thereby acting as major regulators of innate immunity (Almeida-Da-Silva et al., 2023; Sundaram et al., 2024). They are typically composed of a central NACHT (NAIP, CIITA, HET-E and TP1) domain, C-terminal LRRs, and an N-terminal effector domain that mediates downstream signaling (Lechtenberg et al., 2014). Some NLRs, including NLRP3 (NLR family pyrin domain containing 3), assemble inflammasomes that activate caspase-1 and promote maturation of interleukin-1β (IL-1β) and IL-18 as well as pyroptotic cell death (Almeida-Da-Silva et al., 2023; Platnich & Muruve, 2019; Sundaram et al., 2024).

1.2 NLRP3 inflammasome

Inflammasomes are cytoplasmic multiprotein complexes that function as central mediators of innate immune responses. They are assembled in response to microbial infection, cellular stress, or tissue damage and serve as platforms for the activation of inflammatory caspases (Broz & Dixit, 2016; Guo et al., 2015; Latz et al., 2013).

Inflammasomes consist of a sensor protein, the adaptor protein ASC (apoptosis-associated speck-like protein containing the caspase activation and recruitment domain [CARD]), and pro-caspase-1 (Chan & Schroder, 2019; Latz et al., 2013). Following activation, inflammasomes regulate the maturation and secretion of the pro-inflammatory cytokines IL-1β and IL-18 and can induce pyroptotic cell death (Kelley et al., 2019; Próchnicki et al., 2016). Inflammasome assembly is initiated when sensor proteins detect PAMPS or DAMPs. (Chan & Schroder, 2019; He et al., 2015).

Several inflammasome-forming sensor proteins have been identified, including NLRP1, NLRP3 and NLRC4, proteins absent in melanoma 2 (AIM2), and pyrin (Broz & Dixit, 2016; Kelley et al., 2019). Although these receptors differ in their activation mechanisms and the stimuli they recognize, they share the ability to initiate inflammasome assembly, either by directly recruiting pro-caspase-1 or by doing so through ASC, resulting in caspase-1 activation (Latz et al., 2013; Yao et al., 2024). Among these inflammasomes, NLRP3 has received particular attention because of its ability to respond to a remarkably diverse range of stimuli and its involvement in numerous inflammatory diseases (Guo et al., 2015; Kelley et al., 2019).

1.2.1 Structure and function

NLRP3 (NLR family pyrin domain containing 3) is a cytosolic PRR of the NLR family that senses cellular perturbation rather than a single defined ligand (Chen et al., 2023; Kelley et al., 2019; Swanson et al., 2019). It contributes to host defense against infection, but its dysregulated activation is also implicated in autoinflammatory, metabolic, cardiovascular, and neurodegenerative diseases (Kelley et al., 2019).

NLRP3 is a protein composed of an N-terminal pyrin domain (PYD), a central NACHT ATPase domain, and a C-terminal LRR domain (Chen et al., 2023; Coll et al., 2022). The PYD mediates PYD-PYD interactions with the adaptor protein ASC and is therefore essential for inflammasome assembly (Kelley et al., 2019; Zito et al., 2020). The PYD has a conserved six-helix bundle fold that supports these interactions and has therefore emerged as an attractive inhibitory target (Zito et al., 2020).

The central NACHT domain is the main oligomerization engine of NLRP3. Its ATPase activity is required for structural changes and oligomerization after activation. (Kelley et al., 2019; Swanson et al., 2019). Recent cryo-EM studies (Xiao et al., 2022;

Yu et al., 2024) show that activation involves a large rotation of NACHT subdomains into an ATP-bound open state that supports assembly of the active inflammasome.

The role of the LRR domain appears to be more complex than previously thought. (Kelley et al., 2019). Earlier models proposed that the LRR contributes to autoinhibition by folding back onto the NACHT domain (Swanson et al., 2019). However, newer structural and functional studies indicate that the LRR may be dispensable for some activation steps and does not participate directly in active disc interfaces, even though it contributes to the inactive cage-like conformation and to NEK7-associated regulation (Kelley et al., 2019; Xiao et al., 2022). The LRR domain is therefore best described as a regulatory region that helps maintain NLRP3 in its inactive state and supports interactions with licensing factors, rather than as a simple ligand-binding domain (Kelley et al., 2019).

Upon activation, NLRP3 oligomerizes and nucleates ASC polymerization into a perinuclear ASC speck, which then recruits pro-caspase-1 through CARD-CARD interactions (Swanson et al., 2019). Activated caspase-1 cleaves pro-IL-1β and pro-IL-18 and also cleaves gasdermin D (GSDMD), whose N-terminal fragment forms membrane pores that promote cytokine release and pyroptotic cell death (Coll et al., 2022; Zito et al., 2020).

1.2.2 Activation mechanism

Activation of the NLRP3 inflammasome is generally described by a two-signal mechanism consisting of priming and activation (Yang et al., 2019; Zito et al., 2020). The priming step is induced when PRRs, particularly TLRs, detect PAMPs (e.g. LPS) or DAMPs (e.g. ATP) and activate NF-κB, thereby increasing the expression of NLRP3 and pro-IL-1β. Priming also promotes post-translational modifications that enable subsequent NLRP3 activation, rather than simply increasing protein abundance (Chen et al., 2023; Kelley et al., 2019; Zito et al., 2020).

The second signal, activation, can be triggered by a broad range of DAMPs and that leads to inflammasome assembly (Yang et al., 2019; Zito et al., 2020). NLRP3 responds to a broad range of structurally unrelated stimuli, including extracellular ATP, microbial toxins such as nigericin, amyloid fibrils, uric acid crystals, nanoparticles, and other danger-associated perturbations (Coll et al., 2022; Swanson et al., 2019).

Because these agonists are so diverse, NLRP3 is generally thought to sense shared cellular stress signals rather than binding each agonist directly (Kelley et al., 2019).

Among these shared signals, potassium efflux is the most consistently supported upstream event (Y. He et al., 2016). Lower intracellular K+ promotes a conformational change in NLRP3 that precedes inflammasome assembly. The region between the PYD and NACHT domains, including the FISNA-associated segment, appears to be important for linking this ionic change to NLRP3 activation (Xiao et al., 2022). Extracellular ATP is one known trigger of this pathway through P2X7-dependent K+ efflux (Chen et al., 2023; Y. He et al., 2016).

NIMA-related kinase 7 (NEK7) is a key licensing factor downstream of potassium efflux, but the exact species dependence of its role is worth noting (Zito et al., 2020). Structural studies have shown that NEK7 binds to NLRP3 and promotes its transition from an inactive to an active conformation (Y. He et al., 2016). However, one review notes that in human macrophages NEK7 appears to function in priming rather than the activation step itself, and that other human-specific factors such as NLRP11 may contribute (Xu & Núñez, 2022).

Additional pathways including mitochondrial dysfunction, mitochondrial ROS (reactive oxygen species), oxidized mitochondrial DNA release, and lysosomal rupture also contribute to NLRP3 activation (Chen et al., 2023; Kelley et al., 2019). Recent work by Mun et al. (2025) further supports a mechanistic link between mitochondrial stress and inflammasome priming, showing that mitochondrial ROS and DNA release can activate a cGAS-STING-NF-κB axis that increases NLRP3 expression and IL-1β secretion. These pathways appear to converge on conformational and spatial changes that enable NLRP3 oligomerization, ASC recruitment, and caspase-1 activation rather than representing wholly separate endpoint mechanisms (Xiao et al., 2022; Yu et al., 2024).

1.3 NLRP3 gain-of-function diseases

1.3.1 Cryopyrin-associated periodic syndromes

Cryopyrin-associated periodic syndromes (CAPS) are a group of rare monogenic autoinflammatory diseases caused by gain-of-function variants in the *NLRP3* gene. CAPS was named after cryopyrin, an earlier term for the NLRP3 protein (Chen et al.,

2023; Molina-López et al., 2024). CAPS are inherited in an autosomal dominant manner and belong to the broader class of autoinflammatory disorders, which are characterized by recurrent or persistent inflammation in the absence of infection or a classical autoimmune response (Alejandre et al., 2014). Clinically, CAPS consist of three overlapping phenotypes with increasing severity: familial cold autoinflammatory syndrome (FCAS), Muckle–Wells syndrome (MWS), and neonatal-onset multisystem inflammatory disease (NOMID), also termed chronic infantile neurologic cutaneous articular syndrome (CINCA) (Coll et al., 2022; Molina-López et al., 2024). Common symptoms of these syndromes include recurrent fever, urticarial rash, arthritis, ocular inflammation, hearing loss, and central nervous system impairment (Alejandre et al., 2014; Booshehri & Hoffman, 2019).

1.3.2 NLRP3 in CAPS

CAPS are a disease of NLRP3 inflammasome dysregulation (Coll et al., 2022; Kelley et al., 2019). In CAPS, pathogenic *NLRP3* variants lower the activation threshold of the inflammasome, resulting in excessive or inappropriate inflammasome activation and sustained inflammatory cytokine release, especially IL-1β (Alejandre et al., 2014; Booshehri & Hoffman, 2019). This mechanistic link explains why NLRP3 has attracted particular attention among inflammasome pathways, as its broad sensitivity to cellular stress is coupled to a clear monogenic disease phenotype when regulation fails (Kelley et al., 2019; Zito et al., 2020).

Most CAPS-associated variants are located in exon 3/NACHT (NOD) domain of *NLRP3* (Booshehri & Hoffman, 2019; Kelley et al., 2019). In canonical signaling, NLRP3 oligomerization depends on the ATPase activity of the NACHT domain and recruitment of the adaptor ASC through PYD-PYD interactions (Kelley et al., 2019). In CAPS, however, mutant NLRP3 inflammasome may exhibit a reduced requirement for priming and activation signals compared with wild-type NLRP3 and, in some settings, can promote inflammasome assembly without the conventional second activation signal (Alejandre et al., 2014; Booshehri & Hoffman, 2019).

This lowered activation threshold is reflected in patient leukocytes, which show increased caspase-1 cleavage, IL-1β release, and pyroptosis after LPS stimulation without ATP (Booshehri & Hoffman, 2019). More recent evidence suggests that some CAPS-associated variants promote spontaneous inflammasome activation, leading to

basal GSDMD cleavage, IL-18 release, and pyroptotic cell death even in the absence of the usual priming signal, although these mutant inflammasomes remain responsive to NF-κB signaling (Molina-López et al., 2024). Because active caspase-1 processes pro-IL-1β and pro-IL-18, and cleaves GSDMD, CAPS-associated inflammasome dysregulation promotes both cytokine release and pyroptotic inflammatory cell death (Kelley et al., 2019; Molina-López et al., 2024). The resulting excess of IL-1β is strongly implicated in disease pathogenesis, consistent with the marked clinical efficacy of IL-1-targeted therapy in CAPS (Alejandre et al., 2014; Booshehri & Hoffman, 2019).

1.4 Cornea and ocular immune regulation

1.4.1 Corneal anatomy

Cornea is a transparent avascular tissue that forms the outer layer of the eye. It protects the internal structures of the eye and provides about two-thirds of the eye's refractive power (Eghrari et al., 2015; Meek & Knupp, 2015; Sridhar, 2018). The human cornea consists of five layers: the epithelium, Bowman layer, stroma, Descemet's membrane, and the endothelium (Beuerman & Pedroza, 1996; DelMonte & Kim, 2011).

The epithelium covers about 10 % of the corneal thickness and it is a nonkeratinized, stratified aquamous epithelium (Beuerman & Pedroza, 1996). It creates the first barrier to the outside environment (DelMonte & Kim, 2011), and its function is to provide a smooth, regular surface together with the overlying tear film (Sridhar, 2018).

Bowman layer (or Bowman membrane) is not an actual membrane, but rather the acellular condensate of the most anterior part of the stroma. It is a smooth layer that helps the cornea maintain its shape (DelMonte & Kim, 2011).

The stroma covers roughly 80 to 85 % of the cornea's thickness, and it is the structural framework of the cornea. Because of its precise organization of stromal fibers and extracellular matrix (ECM), the stroma is characteristically transparent. The major cell type of the stroma is keratocytes, which are involved in maintaining the ECM environment. (DelMonte & Kim, 2011; Sridhar, 2018).

Beneath the stroma, lining the posterior cornea, there lies Descemet's membrane (Meek & Knupp, 2015). It is a thick basal lamina that is secreted by the

endothelium. Descemet's membrane is composed of an anterior banded portion and a posterior non-banded portion (Beuerman & Pedroza, 1996).

The most posterior layer of the cornea is the endothelium. It is a monolayer, a honeycomb-like mosaic structure (DelMonte & Kim, 2011), and it transports water from the stroma into the anterior chamber of the eye. This movement of water causes the stroma to swell, and this is necessary for maintaining the cornea's transparency (Tuft & Coster, 1990).

1.4.2 Ocular immune privilege

Ocular immune privilege describes the capacity of the eye to limit local immune and inflammatory responses to preserve vision (Wu et al., 2024; Zhou & Caspi, 2010). This protection is mediated by a combination of physical barriers, local inhibitory signals, and systemic regulatory mechanisms, but it is not absolute and remains incompletely understood (Zhou & Caspi, 2010).

In the cornea, these principles are shaped by the need to maintain transparency in a tissue that is, as mentioned, avascular, highly innervated, and continuously exposed to environmental challenges (Downie et al., 2023). Corneal immune privilege is best understood not as immune absence, but as tightly regulated local immunity involving barrier defenses, inhibitory microenvironmental signals, and resident immune cells that preserve tissue clarity while limiting collateral inflammatory damage (Downie et al., 2023; Taylor & Ng, 2018).

However, this balance can fail when barrier integrity is disrupted, neuroimmune signaling is altered, or innate sensing pathways become excessively activated, leading to amplified cytokine production, leukocyte recruitment, and tissue injury (Alenezi et al., 2024; Prieto-Nevárez et al., 2026). Among these pathways, the NLRP3 inflammasome is particularly relevant because it links damage and stress sensing to caspase-1 activation, IL-1β and IL-18 maturation, pyroptosis, and neutrophil-driven corneal inflammation (Ge et al., 2024; Shimizu et al., 2019). Although NLRP3 contributes to host defense and tissue homeostasis, its abnormal activation has been implicated in multiple corneal diseases, including infectious keratitis and dry eye disease, providing a mechanistic framework for tissue-restricted corneal autoinflammation (Ge et al., 2024; Mandell et al., 2022).

1.5 Keratitis fugax hereditaria

1.5.1 Clinical characteristics and epidemiology

Keratitis fugax hereditaria (KFH, MIM 148200) is an autosomal dominant disease predominantly affecting the cornea (Ruusuvaara & Setälä, 1987; Turunen et al., 2018; Valle, 1966). The disease is prevalent in Finland but is presumed to occur also in Sweden (Immonen et al., 2025). KFH is characterized by recurrent episodes of unilateral ocular pain, photophobia, and pericorneal injection. The episodes usually last for 1 to 3 days, but the vision can remain blurry for several weeks. During these acute attacks, the corneal stroma is invaded by inflammatory cells. Acute attacks recur at a mean frequency of 3 to 5 episodes per year, and the disease onset is usually between ages 6 and 20 {Turunen, Joni A., 2020; Turunen, Joni A., 2018}. *In vivo* corneal confocal microscopy studies have suggested that recurrent attacks may lead to structural alterations in the cornea and eventually to the formation of permanent corneal opacities, which can result in reduced vision (Turunen et al., 2020).

KFH was first described by the Finnish ophthalmologist Olavi Valle in 1964 (Valle, 1966), yet diagnosis of the disease was often delayed. The disease was initially called keratitis fugax hereditaria. Later, the name keratoendotheliitis fugax hereditaria was used because early examinations suggested that the corneal endothelium was involved (Ruusuvaara & Setälä, 1987). More recent *in vivo* corneal confocal microscopy and histopathology findings show that the main disease process is in the anterior and middle corneal stroma. The endothelium is not clearly affected. Therefore, the name keratitis fugax hereditaria better describes the disease (Turunen et al., 2020; Turunen et al., 2018).

1.5.2 Genetic background and diagnosis

KFH is caused by a heterozygous pathogenic *NLRP3* variant c.61G>C, p.(Asp21His), in which guanine is replaced by cytosine at nucleotide position 61, resulting in the substitution of aspartic acid with histidine at amino acid position 21 (Immonen et al., 2025; Kawan et al., 2024; Turunen et al., 2020). The NLRP3 gene encodes NLRP3, a key component of the NLRP3 inflammasome, an innate immune signaling complex discussed in Chapter 1.2. The identification of this variant established KFH as an

autoinflammatory disorder and expanded the spectrum of NLRP3-associated diseases (Turunen et al., 2018). Most CAPS-associated variants in *NLRP3* lie in exon 3, which encodes the NACHT (NOD) domain (Kivelä, 2022; Moltrasio et al., 2022), whereas the KFH-causing c.61G>C, p.(Asp21His) variant lies in exon 1 and falls within the pyrin (PYD) domain (Turunen et al., 2018). This positional difference suggests that KFH may activate *NLRP3* through a mechanism distinct from many NACHT-domain CAPS variants, potentially involving altered PYD-mediated interaction with ASC, although direct mechanistic proof remains limited (Feng et al., 2025; Turunen et al., 2018)

The genetic cause of KFH was identified in 2018, which assisted in facilitating the diagnostic process (Turunen et al., 2018). Despite this, the condition has not yet gained widespread recognition among clinicians in Finland (Immonen et al., 2025). A recent study concerning the errors and delays in the diagnosis of KFH (Immonen et al., 2025) showed that KFH can relatively easily be misdiagnosed with other anterior eye conditions. For example, out of 38 patients, 79 % had been misdiagnosed with acute anterior uveitis or anterior chamber cells. This highlights the need for better understanding and knowledge of the disease, even for clinicians.

The identification of the genetic cause of KFH provided important insight into the pathogenesis of the disease, linking the disorder to be the fourth member of CAPS. This discovery expanded the understanding of KFH from an isolated corneal disorder into a disease associated with a pathogenic *NLRP3* variant with dysregulated inflammasome activation (Kawan et al., 2024; Turunen et al., 2018).

1.5.3 Current understanding of disease mechanisms

IL-1β production mediated by the NLRP3 inflammasome has been investigated in KFH. In healthy controls, activation of the NLRP3 inflammasome typically requires both a priming signal, such as LPS, and a secondary activation signal to induce cytokine release (Kawan et al. 2024). A recent study by Kawan et al. (2024) demonstrated that following LPS priming, PBMCs (peripheral blood mononuclear cells) from KFH patients showed a lower threshold for IL-1β secretion than healthy controls. Notably, in PBMCs from patients with frequent KFH symptoms, LPS priming alone was able to trigger substantial IL-1β secretion, whereas patients experiencing occasional attacks showed a subtler release (Kawan et al., 2024). These findings suggest that the *NLRP3*

c.61G>C is a gain-of-function variant, causing a reduced threshold to NLRP3 inflammasome activation and IL-1β release (Kawan et al., 2024). The cellular events linking increased NLRP3 activity to corneal inflammation remain incompletely understood.

The authors of the 2024 study (Kawan et al., 2024) explicitly note that it remains to be identified what triggers the periodic attacks, why KFH is specific to the cornea, and what molecular mechanisms underlie differences in disease severity between patients. Currently, no disease-specific treatment for KFH exists. Topical glucocorticoids, such as prednisolone, are frequently used to reduce inflammation during acute attacks and have been shown to decrease IL-1β secretion in patient-derived cells (Kawan et al., 2024). Development of an *in vitro* disease model for KFH would allow further investigation of the molecular mechanisms underlying inflammasome activation in this disorder and could support the identification of novel treatment strategies.

1.6 Functional disease modeling

1.6.1 THP-1 cells

THP-1 is a human monocytic leukemia cell line, derived from the peripheral blood of an acute monocytic leukemia patient. The cell line is widely used as an *in vitro* model to study inflammatory responses (Bosshart & Heinzelmann, 2016; Chanput et al., 2014). Like primary human monocytes, THP-1 cells express PRRs that recognize PAMPs and DAMPs, including LPS (Auwerx, 1991; Chanput et al., 2014). Upon LPS stimulation, THP-1 cells activate pro-inflammatory signaling pathways, particularly through TLR4, leading to the induction of inflammatory mediators and inflammasome-related proteins such as NLRP3 and pro-IL-1β (Chanput et al., 2014; Yao et al., 2024). THP-1 cells' widespread adoption reflects practical advantages over primary human monocytes, including continuous availability, ease of cryopreservation, experimental reproducibility and the avoidance of donor-to-donor variation (Chanput et al., 2014).

The suspension growth of THP-1 cells is particularly useful for experiments requiring a relatively uniform human monocyte population. The cells can be examined in an undifferentiated state or adapted to macrophage-like experimental systems when required differentiation with phorbol 12-myristate 13-acetate (PMA) is an optional

approach used in some studies (Chanput et al., 2014; Daigneault et al., 2010). In addition to their established use in inflammasome research, THP-1 cells provide a robust platform for genetic manipulation, including CRISPR-Cas9 gene editing (Pinaud & Zamborlini, 2025). Their capacity for clonal expansion following single-cell sorting (Wang et al., 2013) further supports their use in the generation of stable cell models carrying disease-associated variants. For these reasons, THP-1 cells were selected as the experimental model for this study.

1.6.2 CRISPR-Cas9 gene editing

The clustered regularly interspaced short palindromic repeats (CRISPR)-CRISPR-associated protein 9 (Cas9) system is a genome-editing technology adapted from the adaptive immune system of bacteria and archaea (Doudna & Charpentier, 2014; Jiang & Doudna, 2017). In nature, CRISPR loci store fragments of foreign DNA (deoxyribonucleic acid) derived from invading viruses, allowing Cas proteins to recognize and eliminate subsequent infections (Hille & Charpentier, 2016). For genome engineering applications, the system has been simplified to consist primarily of the Cas9 endonuclease and a single-guide RNA (sgRNA), which directs Cas9 to a complementary genomic DNA sequence through Watson-Crick base pairing (Doudna & Charpentier, 2014). Once the target sequence is recognized adjacent to a protospacer adjacent motif (PAM), Cas9 induces a site-specific double-strand break (DSB) in the DNA. The resulting DNA lesion is then repaired by endogenous cellular repair pathways, enabling targeted genetic modifications (Doudna & Charpentier, 2014; Hille & Charpentier, 2016; Jiang & Doudna, 2017).

CRISPR-Cas systems are divided into two classes based on whether they use a multi-subunit effector module (Class 1) or single effector protein (Class 2) (Hille & Charpentier, 2016). Among these, the Class 2 type II CRISPR-Cas9 systems have become one of most widely used methods for genome editing (Lander, 2016). This system requires a guide RNA (gRNA) that consists of CRISPR RNA (crRNA) and trans-activating CRISPR RNA (tracrRNA). The gRNA guides a Cas9 nuclease to produce DSBs in the target DNA location (Doudna & Charpentier, 2014; Hille & Charpentier, 2016). The DNA sequence targeted by the gRNA is referred to as the protospacer and is complementary to the crRNA sequence (Jinek et al., 2012). Efficient target recognition requires the presence of a PAM sequence, typically 5′-NGG-3′ (where N is

any nucleotide), immediately adjacent to the target site (Hille & Charpentier, 2016; Jinek et al., 2012). Following PAM recognition and guide RNA binding, Cas9 generates a DSB approximately three nucleotides upstream of the PAM sequence (Lander, 2016).

Following Cas9-induced DSB formation, the targeted DNA lesion is repaired by endogenous cellular pathways, primarily non-homologous end joining (NHEJ) and homology-directed repair (HDR) (Schubert et al., 2021; Yang et al., 2020). NHEJ repairs DNA double-strand breaks by directly joining the broken DNA ends, often resulting in small insertions or deletions (indels), whereas HDR relies on a homologous DNA template to enable precise repair and targeted sequence modification (Liao et al., 2024; Schubert et al., 2021). Because NHEJ is active throughout most of the cell cycle and generally proceeds more rapidly, it is the predominant repair outcome in mammalian cells, while HDR is largely restricted to S/G2 phase and therefore occurs less frequently (Yang et al., 2020). The main strength of HDR-based CRISPR editing is its ability to introduce predefined genetic modifications, including point mutations, sequence corrections, and targeted insertions, which makes it valuable for disease modeling (Liao et al., 2024; Schubert et al., 2021). In a typical HDR-based experiment, cells receive Cas9 either as an expression construct or as a ribonucleoprotein (RNP) complex together with a target-specific gRNA and a donor DNA template (Schubert et al., 2021). The mechanism of CRISPR-Cas9 gene editing is illustrated in Figure 1.

For small mutations or short insertions, the donor template is commonly supplied as a single-stranded oligodeoxynucleotide (ssODN). ssODNs are especially useful for precise small edits because they are simple to synthesize and can support point mutation introduction without the need for plasmid cloning (Schubert et al., 2021). In contrast, larger knock-in events usually require double-stranded or plasmid-based donors with longer homology arms (Liao et al., 2024).

CRISPR-Cas9 has been increasingly used in NLRP3 inflammasome research to investigate both mechanism and therapeutic targeting. For example, genome-wide CRISPR screening identified NEK7 as an essential upstream regulator of NLRP3 activation. In addition, direct CRISPR-Cas9-mediated disruption of NLRP3 has been shown to decrease inflammasome-driven inflammation in several experimental disease models (Schmid-Burgk et al., 2015; Xu et al., 2018).

CRISPR-Cas9 has become an important tool for studying NLRP3 biology, ranging from the identification of inflammasome regulators to the functional

characterization of disease-associated variants. In this project, HDR-mediated gene editing was selected because the objective was to introduce defined disease-associated *NLRP3* variants rather than generate gene-disrupting indels. Therefore, Cas9 RNP complexes were delivered together with locus-specific ssODN donor templates containing the desired sequence alterations. Successful HDR-mediated repair would be expected to introduce either the KFH-associated or CAPS-associated variant into the *NLRP3* locus.

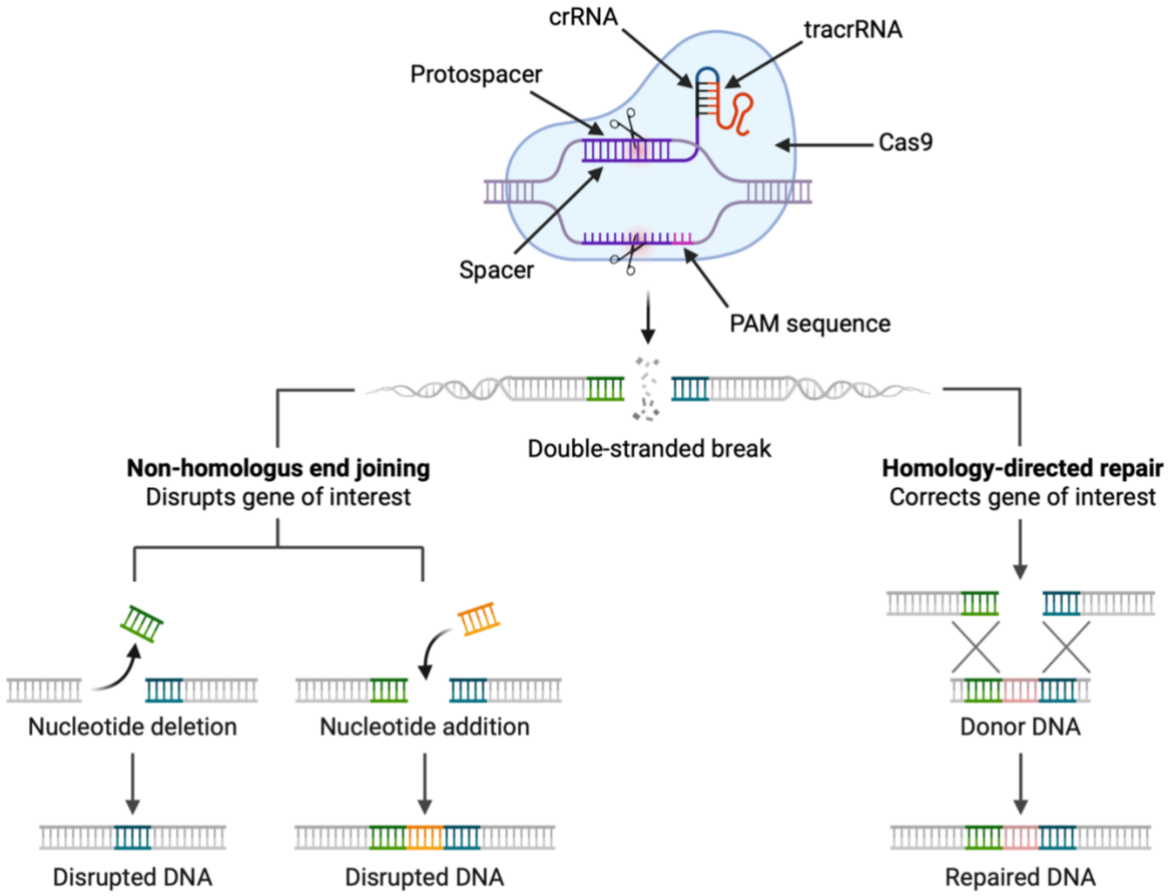

Figure 1: Overview of CRISPR-Cas9 gene editing. Cas9, guided by crRNA and tracrRNA, creates a DSB at a target DNA sequence adjacent to a PAM sequence. The break can be repaired by NHEJ, resulting in insertions or deletions, or by HDR, which uses a donor template to introduce precise sequence changes. Created with BioRender.com.

2 Aim of the thesis

The aim of this thesis was to develop an *in vitro* disease model of keratitis fugax hereditaria (KFH) by introducing the pathogenic *NLRP3* c.61G>C, p.(Asp21His) variant into THP-1 cells using CRISPR-Cas9 gene editing. A secondary aim was to use the generated cell model to investigate how the KFH-associated variant affects inflammasome activation and inflammatory cytokine production. The specific objectives were to:

1. design and implement a CRISPR-Cas9-based strategy for introduction of the *NLRP3* c.61G>C variant
2. identify and validate edited cell clones using molecular methods
3. establish a THP-1 cell model carrying the KFH-associated *NLRP3* variant
4. provide a platform for future studies investigating inflammasome activation and inflammatory signaling associated with KFH.

3 Materials and Methods

3.1 Cell culture

THP-1 (ATCC TIB-202™) cells were cultured in Roswell Park Memorial Institute (RPMI) 1640 Medium (Gibco™) supplemented with 10% fetal bovine serum (FBS) (Gibco™), 1% Penicillin-Streptomycin (Gibco™), 1% GlutaMAX (Gibco™), and 2-Mercaptoethanol (Gibco™, 2198-023) with final concentration of 0.05 mM. Cells were maintained at 37 °C in a humidified incubator with 5% CO_2 (PHCbi CO_2 incubator). Initial cultures were maintained in T25 flasks and subsequently expanded into T75 flasks.

Cell density was monitored regularly using a Cellometer K2 Fluorescent Viability Cell Counter (Nexcelom Bioscience, Manchester, UK). Complete medium change was performed at least every seven days but usually every three days. Cells were passaged when the concentration reached approximately 0.8×10^6 cells/mL and were maintained below 1.5×10^6 cells/mL to preserve optimal growth and viability. All cultures were routinely inspected for morphology and cell density throughout the experimental period.

For single-cell sorting, cells were sorted into 96-well plates containing 100 µL of complete culture medium per well. Every seven days, approximately half of the medium was removed and replaced with fresh medium. Once clonal populations had expanded sufficiently for transfer to larger culture vessels, complete medium changes were performed as described above.

When not used for experiments, cells were cryopreserved in liquid nitrogen. Freezing medium consisted of 90% FBS and 10% Dimethyl Sulfoxide (DMSO) cell culture reagent (MP Biomedicals). Cells were resuspended at 5×10^6 cells/mL in freezing medium, aliquoted into cryovials, and stored at −80 °C overnight in a freezing container before transfer to liquid nitrogen for long-term storage.

3.2 Experimental design

The study was designed to generate and validate CRISPR-Cas9-edited THP-1 cell clones carrying disease-associated *NLRP3* variants. Four experimental groups were

included: a KFH editing group, a CAPS editing group that served as a positive control, a non-targeting control, and an unedited wild-type (WT) control. The composition and purpose of each experimental group are summarized in Table 1. All groups were cultured and processed simultaneously under identical experimental conditions to minimize technical variation.

The experimental workflow included gRNA and donor template design, assembly of CRISPR-Cas9 RNP complexes, electroporation of THP-1 cells, flow cytometry to detect transfected cells, clonal expansion by single-cell sorting, screening of candidate clones by restriction enzyme digestion, and confirmation of selected clones by Sanger sequencing. The overall workflow is illustrated in Figure 4, at the end of this section.

Table 1: Experimental groups included in this study and their intended purpose.

Group	Intended edit	RNP complex	HDR donor	Purpose
KFH	*NLRP3* c.61G>C, p.(Asp21His) at chr1:247418855	Yes	Yes	Generation of validated edited clones for development of a KFH disease model
CAPS	*NLRP3* c.778_780delinsTGG, p.(Arg260Trp) at chr1:247424227 (linked with FCAS and MWS)	Yes	Yes	Positive control for HDR-mediated editing and clone validation
Non-targeting	None	Yes	No	Control for effects of electroporation and CRISPR-Cas9 delivery
WT	None	No	No	Baseline wild-type control

3.3 CRISPR-Cas9

3.3.1 CRISPR-Cas9 target and donor design

HDR donor templates and gRNA with tracrRNA (trans-activating CRISPR RNA) and crRNA (CRISPR RNA) were designed using IDT™ Alt-R™ HDR Design Tool (Integrated DNA Technologies). Target sites were selected within the *NLRP3* gene based on their proximity to the desired knock-in locations and predicted editing efficiency. The targeted *NLRP3* variants and their genomic locations are summarized in Table 1.

Representative outputs from the design tool are shown in Figures 2 and 3. gRNAs were selected based on predicted on-target activity, specificity score, and proximity of the Cas9 cleavage site to the desired variant. Preference was given to guides predicted to introduce DSBs within a few nucleotides of the intended edit to maximize HDR efficiency. HDR single-stranded donor oligodeoxynucleotides (ssODNs) were designed to introduce the desired mutations at the target loci. KFH and CAPS HDR donor templates consisted of 86 and 83 nucleotides, respectively. Both containing 40-nucleotide homology arms upstream and downstream of the intended edit site.

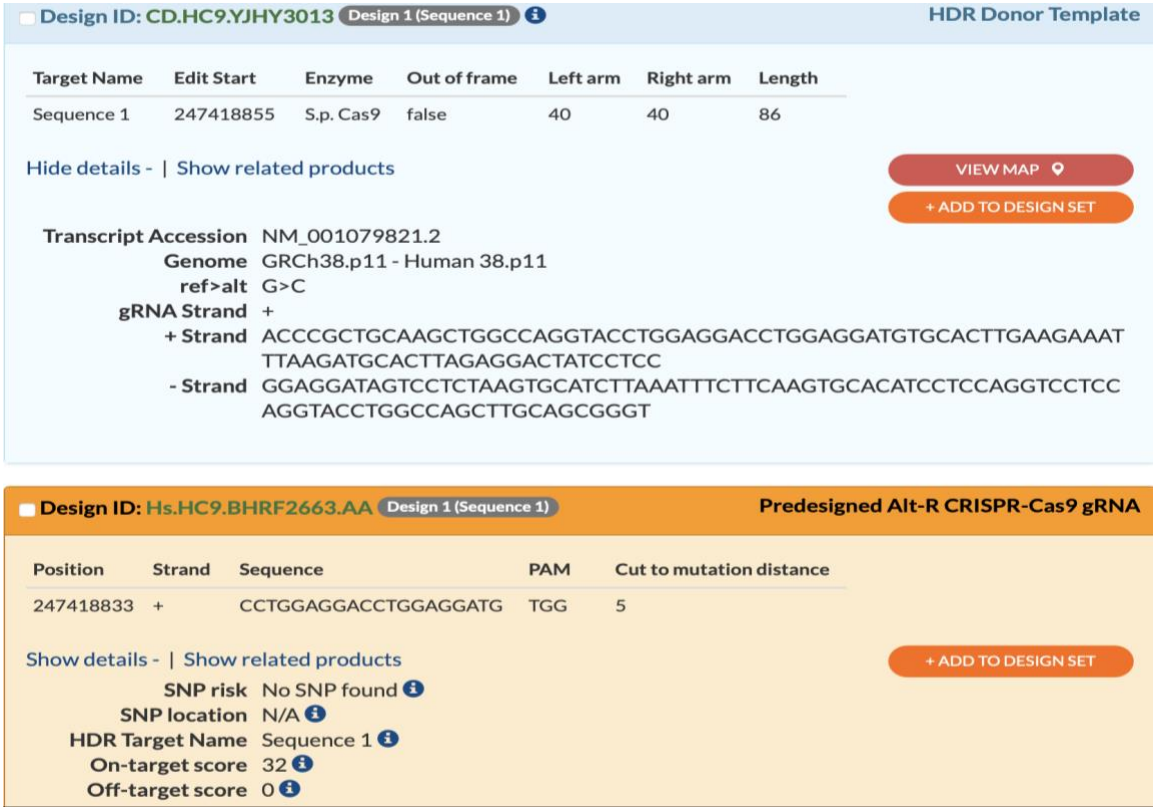

Figure 2: Design of CRISPR-Cas9 reagents for introduction of the KFH-associated *NLRP3* c.61G>C variant. Screenshot from the IDT™ Alt-R™ HDR Design Tool showing the selected gRNA and HDR donor design. The gRNA was predicted to cut 5 bp from the intended edit site and had predicted on-target and off-target specificity scores of 32 and 0, respectively.

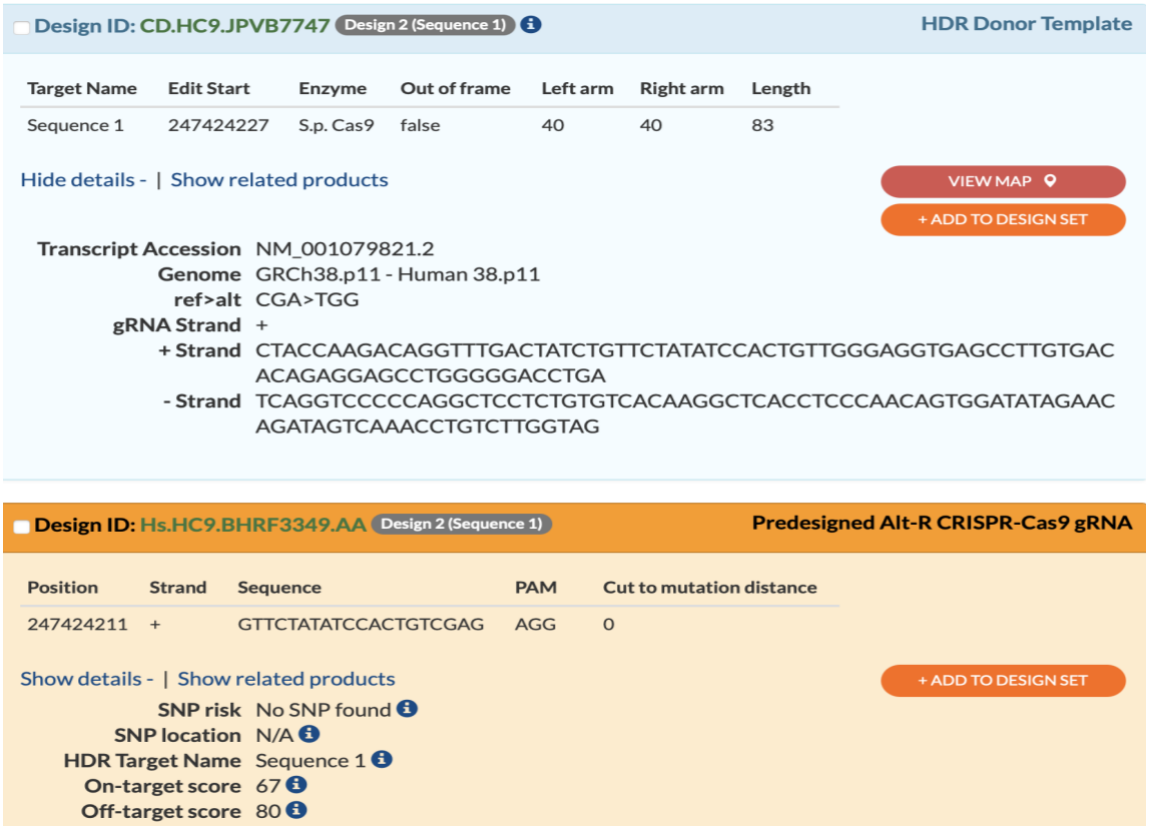

Figure 3: Design of CRISPR-Cas9 reagents for introduction of the CAPS-associated *NLRP3* c.778_780delinsTGG variant. Screenshot from the IDT™ Alt-R™ HDR Design Tool showing the selected gRNA and HDR donor design. The guide RNA cleavage site coincided with the intended edit position (cut-to-mutation distance 0 bp) and had predicted on-target and off-target specificity scores of 67 and 80, respectively.

3.3.2 CRISPR reagents

Gene editing experiments were performed using the Alt-R™ CRISPR-Cas9 system (Integrated DNA Technologies). The editing components included Alt-R S.p. HiFi Cas9 Nuclease V3, locus-specific Alt-R CRISPR-Cas9 crRNAs, Alt-R tracrRNA labeled with ATTO™ 550 fluorescence dye, and ssODN HDR donor templates. A non-targeting control crRNA was used as a negative control. All oligonucleotides were resuspended in nuclease-free IDTE buffer and stored at −20°C until use.

3.3.3 gRNA annealing and RNP complex formation

gRNA complexes were prepared by annealing crRNA and tracrRNA at 1:1 molar ratio according to the manufacturer's recommendations (Table 2). The mixture was heated at 95 °C for 5 min and allowed to cool to room temperature. RNP complexes were assembled from annealed gRNA, Alt-R™ S.p. HiFi Cas9 Nuclease V3, and Neon™ Resuspension Buffer R as shown in Table 3. The assembled RNP complexes were incubated for 15 min at room temperature prior to use and subsequently maintained at 4 °C until electroporation. No HDR enhancer or electroporation enhancer was included in the protocol.

Table 2: gRNA annealing reaction

Component	Amount (µL)
200 µM crRNA	3
200 µM tracrRNA with ATTO™ 550	3
Total volume	6 (100 µM)

Table 3: RNP complex reaction

Component	Amount (µL)
gRNA (100 µM)	3
Cas9 enzyme (62 µM)	3
Buffer R	3
Total volume	9 (20.7 µM)

3.4 Electroporation

3.4.1 Preparing cells for electroporation

THP-1 cells were maintained in culture for approximately one month prior to gene editing to ensure stable growth and optimal cell health. Cells in the logarithmic growth phase were collected and washed once with phosphate-buffered saline (PBS), followed by centrifugation (Heraeus Instruments, Megafuge 1.0) at 400 × g for 8 min at room temperature. Cell pellets were resuspended in Neon Resuspension Buffer R to a final concentration of 2×10^7 cells/mL, corresponding to 2×10^6 cells per 100 µL reaction.

3.4.2 Electroporation procedure

For editing reactions (KFH and CAPS), transfection mixtures consisted of RNP complexes, HDR ssODNs, and THP-1 cells suspended in Neon™ Resuspension Buffer R. Component volumes and final concentrations are shown in Table 4. For non-targeting control, only RNP complex and cell suspension were used for transfection mix and ssODN was replaced with an equivalent volume of Buffer R.

Table 4: Transfection mix for electroporation

Component	Amount (µL)
RNP complex (20.7 µM) HDR ssODN (200 µM) Cell suspension	3 (0.56 µM) 1 (0.65 µM) 100
Total volume	104

To facilitate pipetting, an additional 15 µL of Buffer R was added to each reaction mixture. Electroporation was performed using the Neon™ Transfection System (Invitrogen) with a single pulse of 1700 V for 20 ms. Immediately after electroporation, cells were transferred to pre-warmed RPMI 1640 medium supplemented with FBS and GlutaMAX™ (without antibiotics) and incubated overnight at 37 °C containing 5 % CO_2.

To provide backup populations for subsequent experiments, two independent electroporations were performed using the KFH-specific RNP complex and ssODN donor template, and two independent electroporations were performed using the CAPS-specific RNP complex and ssODN donor template. These generated the KFH1/KFH2 and CAPS1/CAPS2 populations used in later stages of the study.

3.5 Fluorescence-Activated Cell Sorting (FACS)

Fluorescence-activated cell sorting (FACS) is a flow cytometry technique that enables the identification and isolation of cell populations based on their light-scattering and fluorescence properties (Herzenberg et al., 2002). Forward scatter (FSC) and side

scatter (SSC) parameters were used to distinguish viable single cells from debris and cell aggregates through gating.

In this study, FACS was to sort THP-1 cells positive for ATTO™ 550 fluorescence. The tracrRNA component of the CRISPR-Cas9 RNP complex was labeled with ATTO™ 550, allowing identification of cells that had taken up the editing complex. Since fluorescence only confirms intracellular delivery of the RNP complex and not successful genome editing, subsequent molecular screening was required to verify introduction of the desired variants. ATTO™ 550-positive cells from the KFH (1 and 2), CAPS (1 and 2), and non-targeting control groups were isolated and expanded in culture. Following recovery and expansion, the KFH2 and CAPS2 populations were cryopreserved as backup stocks. Single-cell sorting was performed for the KFH1 and CAPS1 populations to establish clonal cell lines for downstream screening and validation. Hereafter, KFH1 and CAPS1 are referred to as KFH and CAPS, respectively.

3.5.1 Sample preparation and initial sorting

Approximately 24 h after electroporation, cells were harvested and washed once with PBS. Following centrifugation at 400 × g for 8 min, cells were resuspended in 200 µL PBS and maintained on ice until analysis. Flow cytometric analysis and cell sorting were performed at the Biomedicum Flow Cytometry Unit. Wild-type cells were not subjected to FACS. Following sorting, cells were cultured in complete RPMI 1640 medium and incubated at 37 °C containing 5 % CO_2. Cells were allowed to recover and expand for approximately two weeks before the next sorting.

3.5.2 Single-cell sorting

After cells had recovered and grown from the ATTO-550 sorting, cells of KFH and CAPS were single-cell sorted by FACS into 96-well plates containing complete growth medium (100 µL) and incubated at 37 °C containing 5% CO_2. Single-cell sorting was not performed for the non-targeting control or wild-type groups.

Due to limited clonal outgrowth from the first single-sorting, additional rounds of single-cell sorting were performed using cryopreserved edited KFH1 and KFH1 cell

populations. In total, three sets of 96-well plates were established and monitored for clonal expansion.

3.6 Screening of cultured clones

3.6.1 DNA extraction

Genomic DNA was isolated from expanded single-cell colonies using QuickExtract™ DNA Extraction Solution (Lucigen) according to the manufacturer's instructions. Approximately 1 × 10^6 cells were used for each extraction. DNA concentration and purity were determined using a DeNovix (DS-11 FX+) spectrophotometer. DNA concentrations ranged from 94.6 to 188.1 ng/µL, and all samples were subsequently diluted to a working concentration of 50 ng/µL for downstream applications.

3.6.2 Amplification of DNA

Target regions of the *NLRP3* gene were amplified by polymerase chain reaction (PCR) using genomic DNA extracted from single-cell colonies. Primers were designed to amplify the genomic regions containing the KFH and CAPS variants and were ordered from Sigma-Aldrich. Primer sequences and expected amplicon sizes are shown in Table 5.

Table 5: PCR primers used for amplification of *NLRP3* target regions.

Target	Primer	Sequence (5′→3′)	Amplicon size (bp)
KFH	Forward	AAAAGACTCATCCGTGTGCCG	377
KFH	Reverse	GTCTTCCTTCCACTCACCCCA	377
CAPS	Forward	GTTTGACCCCGATGATGAGC	244
CAPS	Reverse	CTTGTGGATGGGTGGGTTTG	244

PCR reactions were prepared in a final volume of 20 µL. Reaction components are shown in Table 6.

Table 6: PCR reaction mixture.

Reagent	20 µL reaction volume
Milli-Q water	14.9 µL
10x Standard Reaction Buffer with MgCl2 (Biotools)	2 µL
Primer, forward (5 µM)	0.65 µL
Primer, reverse (5 µM)	0.65 µL
dNTP Mix (10 mM) (Thermo Scientific)	0.2 µL
DNA Polymerase (1U/µL) (Biotools)	0.6 µL
DNA (50 ng/µL)	1 µL

PCR was performed using a Bio-Rad C1000 Touch Thermal Cycler. PCR cycling conditions are summarized in Table 7. The CAPS amplification protocol was identical to that used for KFH, except that 35 amplification cycles were performed instead of 34. PCR products were analyzed by electrophoresis (Bio-Rad PowerPac Basic™) on 2 % agarose (Biotop BIO-41025) gels stained with MIDORI Green Advance (Nippon Genetics Europe) and imaged with Nippon Genetics Europe GDS.

Table 7: PCR protocol for KFH.

Step	Temperature	Time	Repeats
Initial denaturation	94 °C	10 min	Once
Denaturation Annealing Extension	94 °C 62 °C 72 °C	45 s 45 s 1 min	34 cycles
Final extension	72 °C	10 min	Once
Cooling	4 °C	Forever	

3.6.3 Restriction digestion

Restriction fragment length analysis was used as an initial screening method to identify candidate edited clones. Following PCR amplification, samples were digested with FastDigest restriction enzymes (Thermo Scientific) selected based on the expected sequence changes introduced by genome editing. For KFH samples, FastDigest Alw44I (#FD0044) was used because successful editing introduced a restriction site,

resulting in cleavage of the PCR product. For CAPS samples, FastDigest TaqI (#FD0674) was used because successful editing disrupted the restriction site, preventing cleavage of the PCR product.

Digestion reactions were prepared according to the manufacturer's instructions in a final volume of 15 µL containing PCR product, 10X FastDigest Green Buffer, restriction enzyme, and Milli-Q water. Alw44I reactions were incubated at 37 °C for 15 min, whereas TaqI reactions were incubated at 65 °C for 15 min. Digested products were analyzed by electrophoresis (Bio-Rad PowerPac Basic™) on 2% agarose (Biotop BIO-41025) gels stained with MIDORI Green Advance (Nippon Genetics Europe) and imaged with Nippon Genetics Europe GDS.

3.6.4 Sanger sequencing

Prior to sequencing, PCR products were purified using ExoSAP-IT™ PCR Product Cleanup Reagent (Thermo Fisher Scientific) to remove residual primers and unincorporated nucleotides. Purification reactions (10 µL of PCR product and 2 µL of ExoSAP-IT) were incubated at 37°C for 30 min, followed by enzyme inactivation at 80°C for 15 min according to the manufacturer's protocol.

Purified PCR products were subjected to cycle sequencing using the BigDye™ Terminator v3.1 Cycle Sequencing Kit (Applied Biosystems) with Bio-Rad C1000 Touch Thermal Cycler. Sequencing reactions were prepared in a final volume of 10 µL according to the manufacturer's recommendations. The composition of the reaction mixture is shown in Table 8. Cycle sequencing was subsequently performed using the conditions summarized in Table 9.

Table 8: Reaction mixture for cycle sequencing.

Reagent	10 µL reaction volume
Milli-Q water	5.10 µL
BigDye Terminator V1.1. V3.1 5x Sequencing Buffer	1.75 µL
Primer (5 µM) (forward and reverse separately)	0.65 µL
BigDye Terminator V3.1 Cycle Sequencing RR-100	0.50 µL
Cleaned PCR product	2.0 µL

Table 9: Cycle sequencing protocol.

Step	Temperature	Time	Repeats
Initial denaturation	96 °C	1 min	Once
Denaturation Annealing Extension	96 °C 58 °C 60 °C	10 s 10s 4 min	28 cycles
Cooling	4 °C	Forever	

Sanger sequencing was performed at the Institute for Molecular Medicine Finland FIMM Genomics unit supported by HiLIFE and Biocenter Finland. Sequencing results were analysed to confirm the presence of the intended *NLRP3* edits in KFH and CAPS samples. In addition, wild-type samples with KFH and CAPS primers were sequenced for reference and validation.

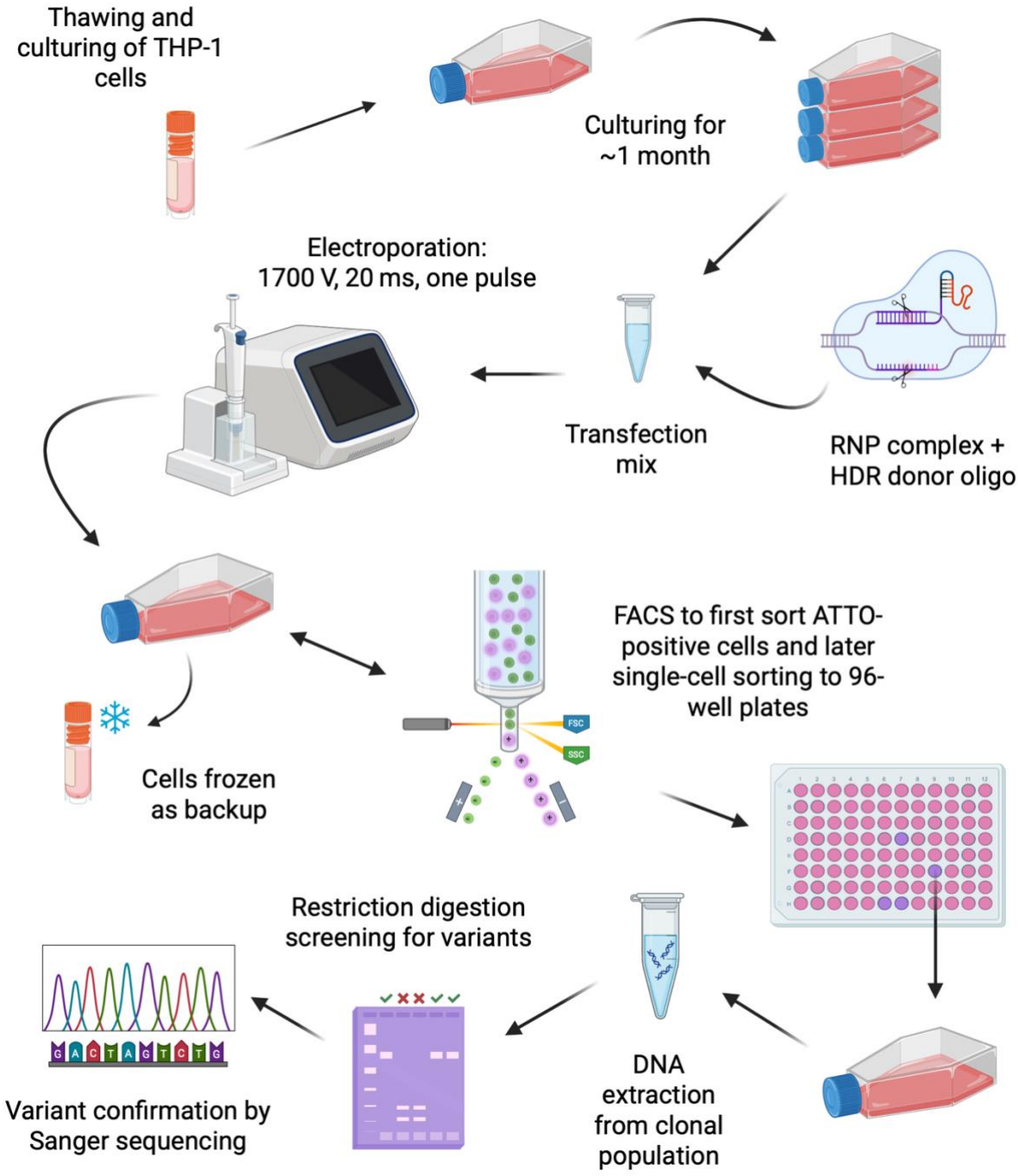

Figure 4: Workflow of the project. Created with BioRender.com.

4 Results

4.1 Nature of THP-1 cell growth and maintenance

THP-1 cells recovered successfully after thawing, and they mostly displayed a characteristic suspension growth pattern throughout the culture period. Since the cells were first thawed, the live cell count increased from 0.333 x 10^6 cell/mL to 0.935 x 10^6 cells/mL, and the cell viability increased from 60.6 % to 98.2 % within ten days. Overall, cell growth was initially slow after thawing but became exponential after adaptation to culture conditions. No contamination or issues related to culturing were observed during routine maintenance.

Before electroporation and the initial FACS, cells had been growing for almost four weeks, and they had reached the appropriate concentration required for the subsequent steps. After electroporation and FACS, edited cell populations were cultured for approximately two weeks before single-cell sorting. Cell viability exceeded 90 % prior to sorting. After single-cell sorting into 96-well plates, cellular growth was slower than in bulk cultures. Expansion of single-cell clones required approximately 4–5 weeks before transfer to larger culture vessels was possible.

Clonal growth was limited in the first set of plates, with only one viable clone observed in the KFH1 plate and one viable clone in the CAPS1 plate after approximately three weeks of culture. Consequently, additional rounds of single-cell sorting were performed. Clone growth remained low in the following two plate sets, although more clones were obtained than in the first round.

Few KFH clones initially showed successful growth following single-cell sorting in 96-well plates. However, some clones failed to maintain viability during subsequent culture and underwent complete cell death before transfer to larger culture vessels was possible. Representative micrographs of a viable clone and a non-viable clone are shown in Figure 5. In total, two viable KFH clones and three viable CAPS clones showed sufficient growth for downstream screening.

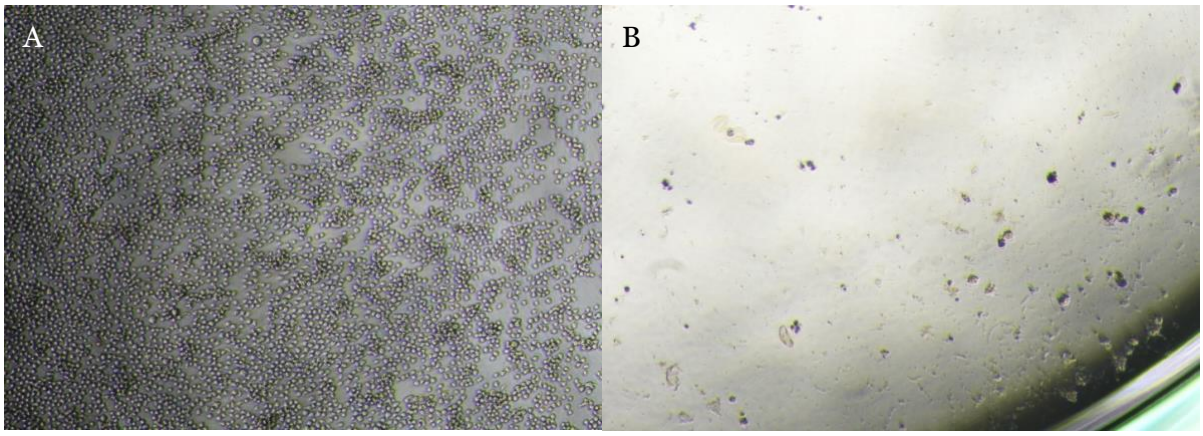

Figure 5: THP-1 single-cell clones growing in a 96-well plate after single-cell sorting. A: Viable KFH cells. B: Non-viable KFH cells. Both clones have been growing for four weeks.

4.2 Fluorescence-Activated Cell Sorting

FACS was performed to assess cell viability and the delivery of CRISPR-Cas9 RNP complexes after electroporation. All sample groups were analyzed using a sequential gating strategy based on cell size and granularity, followed by singlet selection, viability gating, and detection of ATTO™ 550 fluorescence. However, only the non-targeting, KFH1, KFH2, CAPS1, and CAPS2 populations were subjected to fluorescence-based sorting and further culture, as these samples contained the CRISPR-Cas9 components and the ATTO™ 550 fluorescence channel.

Representative gating strategies and ATTO™ 550-positive cell populations are shown in Figures 6–11. In the non-targeting sample, 95.80 % of the analyzed cells were positive for ATTO™ 550 fluorescence (Figure 7). The percentages of ATTO™ 550-positive cells in the KFH1 and KFH2 samples were 83.20 % and 99.56 %, respectively (Figures 8 and 9). Similarly, 99.21 % and 99.13 % of cells in the CAPS1 and CAPS2 samples were ATTO™ 550-positive, respectively (Figures 10 and 11). The high proportion of ATTO™ 550-positive cells in all electroporated populations indicated efficient delivery of the CRISPR-Cas9 RNP complexes into THP-1 cells.

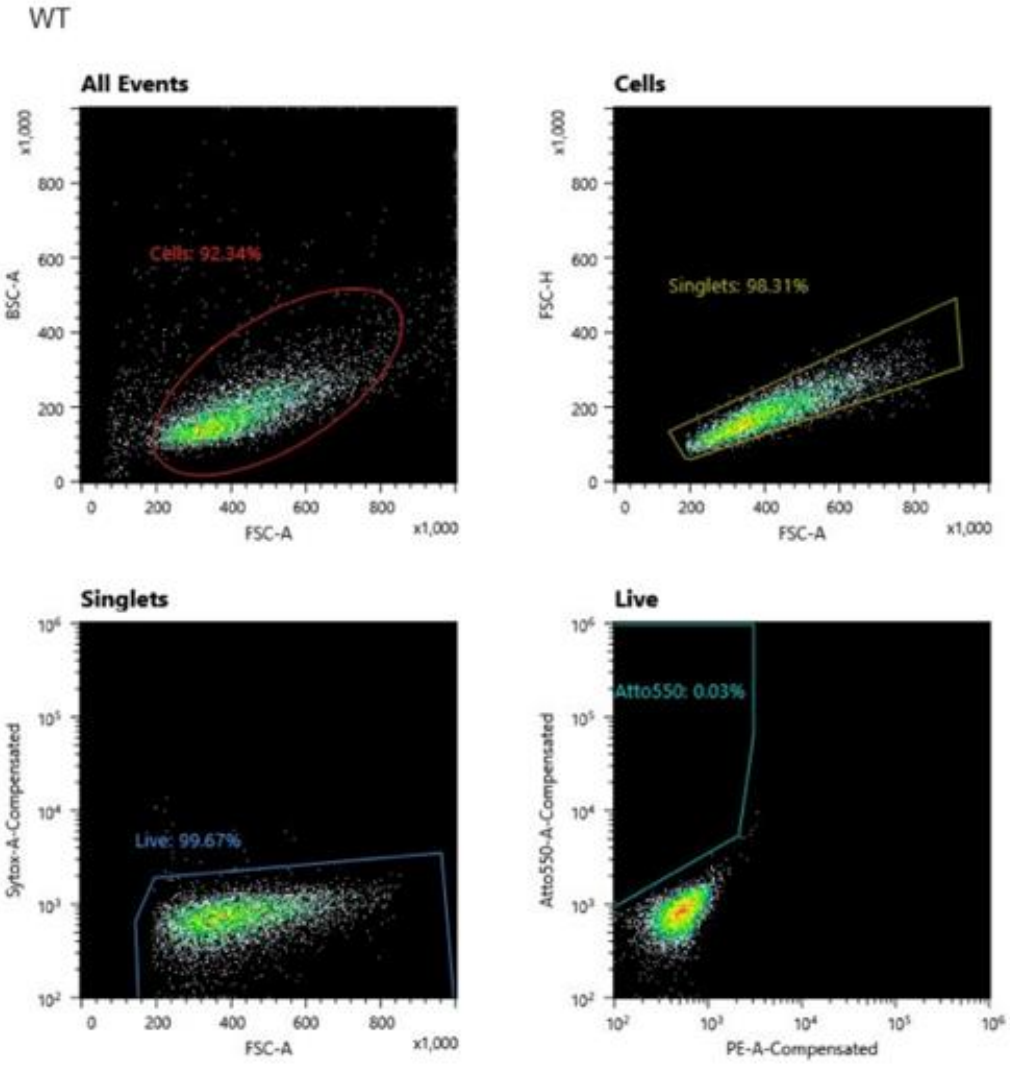

Gates and Statistics

Name	Events	%Parent	%Total	
All Events	6,594	0.00%	100.00%	
Cells	6,089	92.34%	92.34%	
Singlets	5,986	98.31%	90.78%	
Live	5,966	99.67%	90.48%	
Atto550	2	0.03%	0.03%	

Figure 6: FACS plots showing the gating strategy for wild-type (WT) cells. Cell populations were gated sequentially based on size and granularity (FSC-A/BSC-A), singlet discrimination (FSC-A/FSC-H), viability (FSC-A/Sytox-A-Compensated), and Atto550 fluorescence (PE-A-Compensated/Atto550-A-Compensated). The table summarizes the events retained at each gating step.

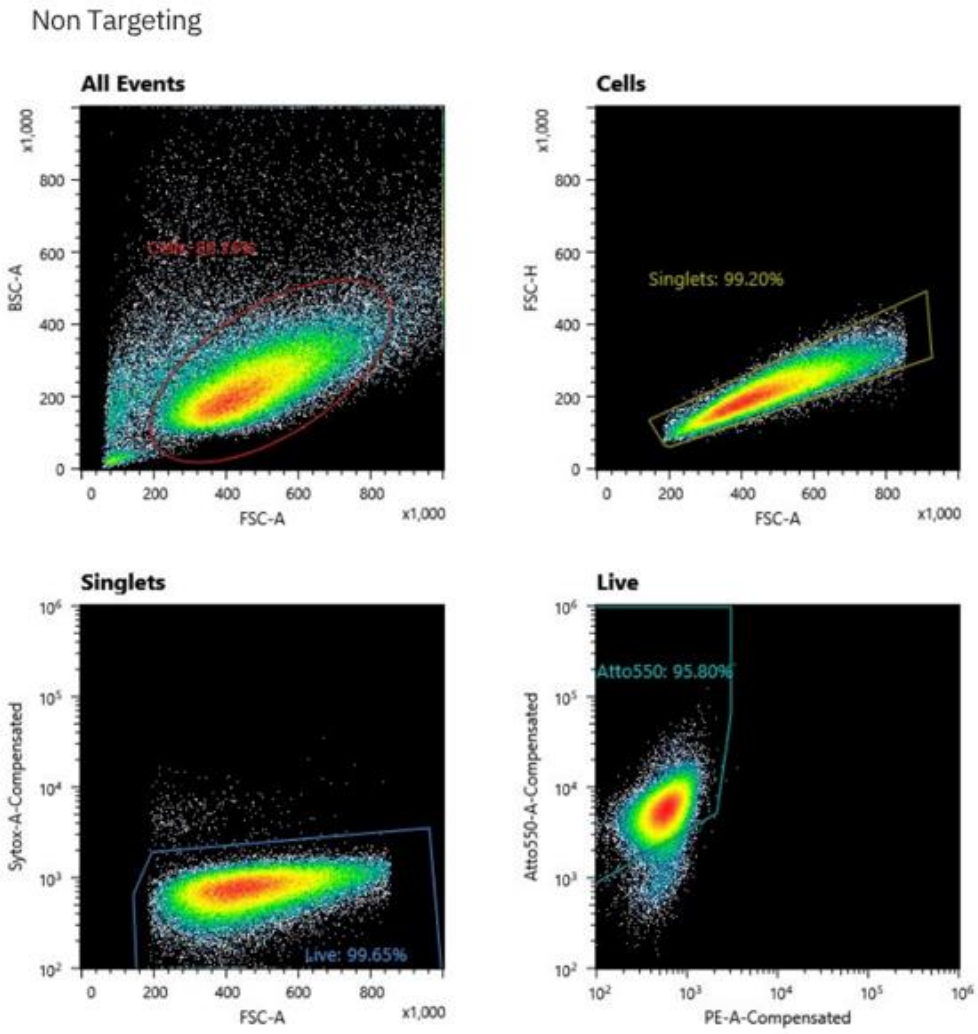

Gates and Statistics

Displaying 100,000 / 115,938 events

Name	Events	%Parent	%Total
All Events	100,000	0.00%	100.00%
Cells	86,159	86.16%	86.16%
Singlets	85,471	99.20%	85.47%
Live	85,171	99.65%	85.17%
Atto550	81,592	95.80%	81.59%

Figure 7: FACS plots showing the gating strategy for non-targeting cells. Cell populations were gated sequentially based on size and granularity (FSC-A/BSC-A), singlet discrimination (FSC-A/FSC-H), viability (FSC-A/Sytox-A-Compensated), and Atto550 fluorescence (PE-A-Compensated/Atto550-A-Compensated). The table summarizes the events retained at each gating step.

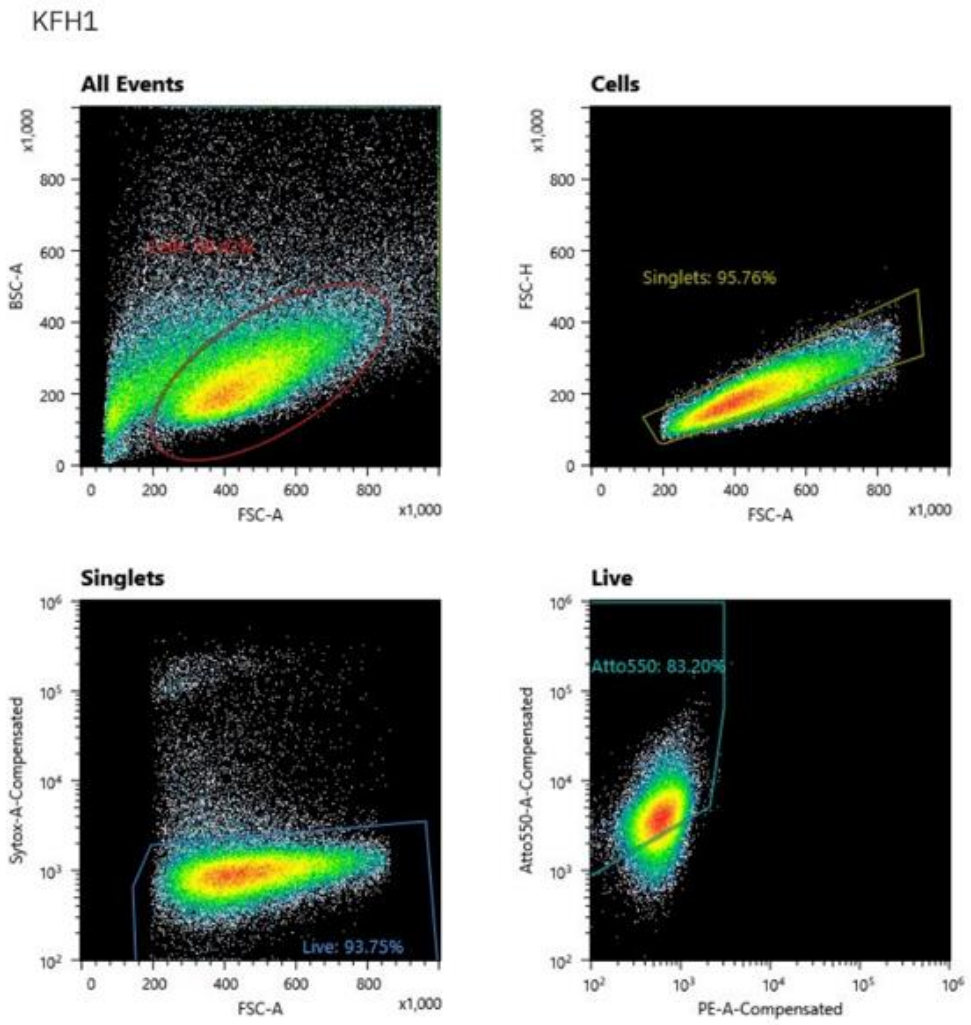

Gates and Statistics

Displaying 100,000 / 142,385 events

Name	Events	%Parent	%Total
All Events	100,000	0.00%	100.00%
Cells	69,421	69.42%	69.42%
Singlets	66,478	95.76%	66.48%
Live	62,322	93.75%	62.32%
Atto550	51,849	83.20%	51.85%

Figure 8: FACS plots showing the gating strategy for KFH1 cells. Cell populations were gated sequentially based on size and granularity (FSC-A/BSC-A), singlet discrimination (FSC-A/FSC-H), viability (FSC-A/Sytox-A-Compensated), and Atto550 fluorescence (PE-A-Compensated/Atto550-A-Compensated). The table summarizes the events retained at each gating step.

KFH2

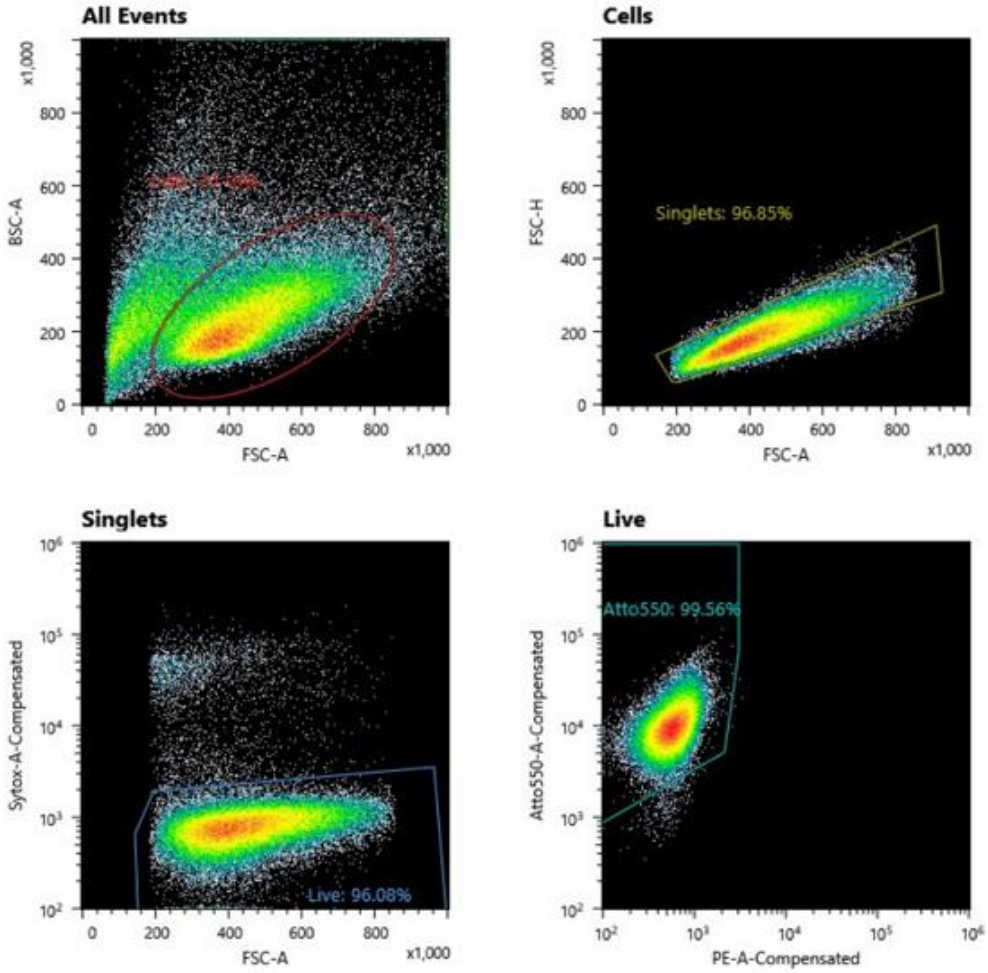

Gates and Statistics Displaying 100,000 / 141,814 events

Name	Events	%Parent	%Total
All Events	100,000	0.00%	100.00%
Cells	70,103	70.10%	70.10%
Singlets	67,894	96.85%	67.89%
Live	65,231	96.08%	65.23%
Atto550	64,945	99.56%	64.95%

Figure 9: FACS plots showing the gating strategy for KFH2 cells. Cell populations were gated sequentially based on size and granularity (FSC-A/BSC-A), singlet discrimination (FSC-A/FSC-H), viability (FSC-A/Sytox-A-Compensated), and Atto550 fluorescence (PE-A-Compensated/Atto550-A-Compensated). The table summarizes the events retained at each gating step.

CAPS1

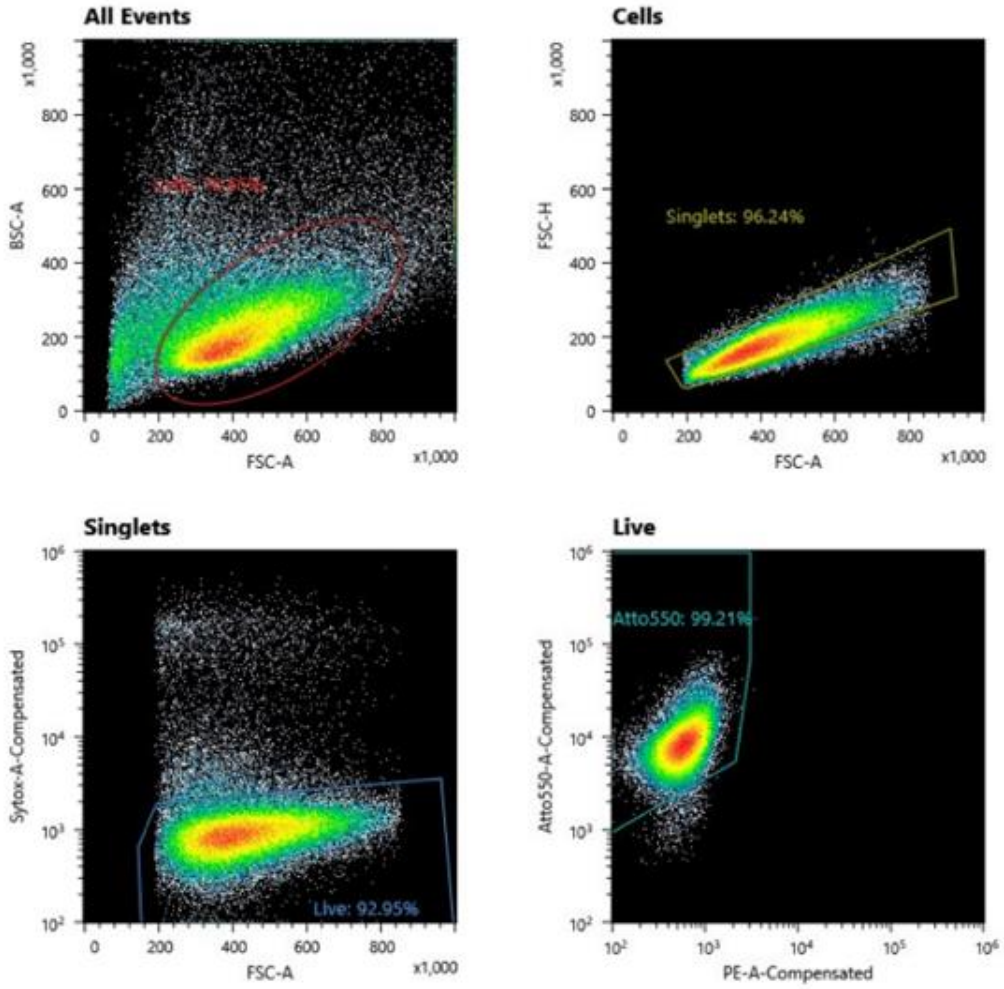

Gates and Statistics

Displaying 100,000 / 126,369 events

Name	Events	%Parent	%Total	
All Events	100,000	0.00%	100.00%	
Cells	78,652	78.65%	78.65%	
Singlets	75,698	96.24%	75.70%	
Live	70,362	92.95%	70.36%	
Atto550	69,808	99.21%	69.81%	

Figure 10: FACS plots showing the gating strategy for CAPS1 cells. Cell populations were gated sequentially based on size and granularity (FSC-A/BSC-A), singlet discrimination (FSC-A/FSC-H), viability (FSC-A/Sytox-A-Compensated), and Atto550 fluorescence (PE-A-Compensated/Atto550-A-Compensated). The table summarizes the events retained at each gating step.

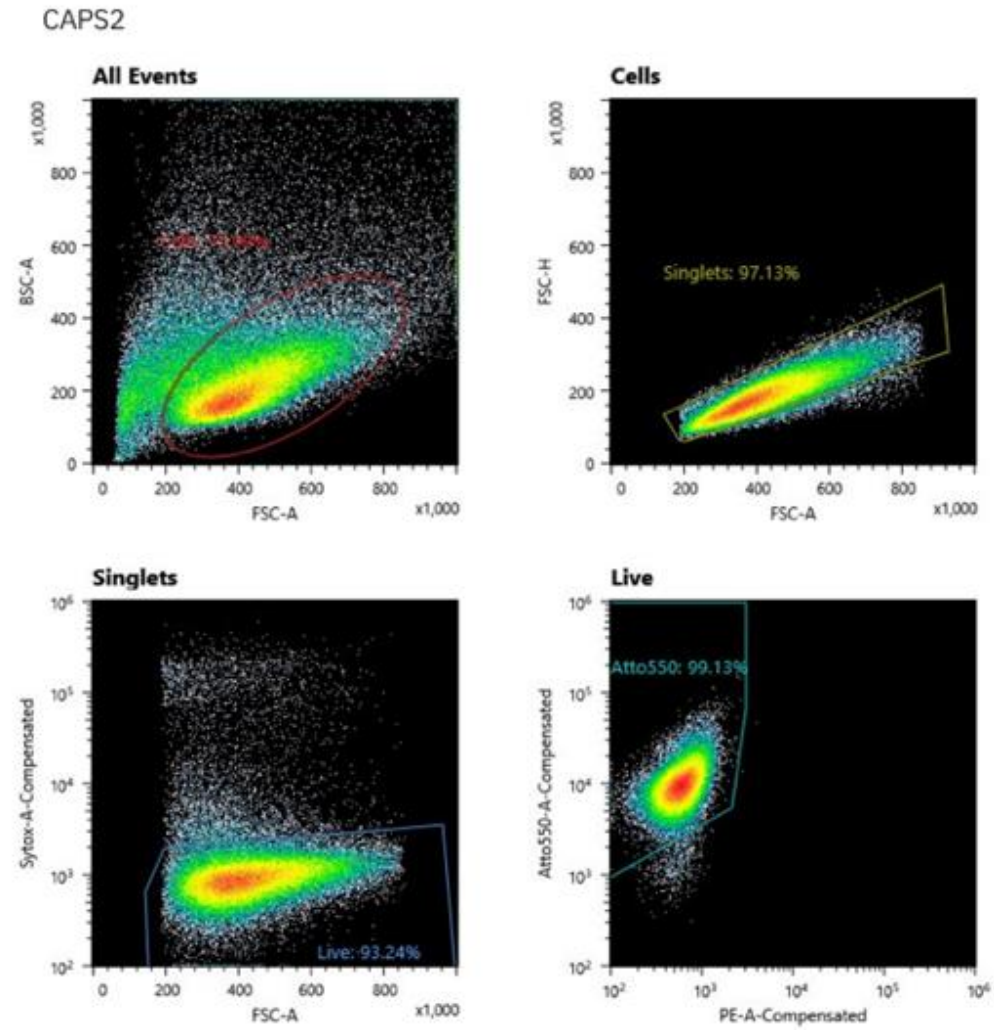

Gates and Statistics

Displaying 100,000 / 132,484 events

Name	Events	%Parent	%Total
All Events	100,000	0.00%	100.00%
Cells	75,092	75.09%	75.09%
Singlets	72,940	97.13%	72.94%
Live	68,010	93.24%	68.01%
Atto550	67,415	99.13%	67.42%

Figure 11: FACS plots showing the gating strategy for CAPS2 cells. Cell populations were gated sequentially based on size and granularity (FSC-A/BSC-A), singlet discrimination (FSC-A/FSC-H), viability (FSC-A/Sytox-A-Compensated), and Atto550 fluorescence (PE-A-Compensated/Atto550-A-Compensated). The table summarizes the events retained at each gating step.

4.3 Assessing the CRISPR edit in THP1 cells

Restriction digestion was used as an initial screening method to identify clones that might contain the desired KFH and CAPS variants. PCR products from the expanded clones were digested with the appropriate restriction enzymes and analyzed by agarose gel electrophoresis. All gels were run with the KFH or CAPS samples, wild-type controls, and negative controls without the restriction enzyme.

For the two KFH clones analyzed by restriction digestion, one clone showed a digestion pattern consistent with the wild-type sequence (Figure 12). All four samples produced a single band at approximately 377 bp, corresponding to the expected PCR product size. No additional bands indicative of restriction enzyme cleavage were observed in the E62 sample, suggesting that the introduced mutation was not present or was not detectable by this screening method.

The second clone (E6) showed a digestion pattern that differed from the wild-type control (Figure 13). Three bands were visible on the gel, while the wild-type sample produced a single band at approximately 377 bp. To ensure accurate identification of edited clones, both KFH samples were analyzed further by Sanger sequencing regardless of their restriction digestion patterns.

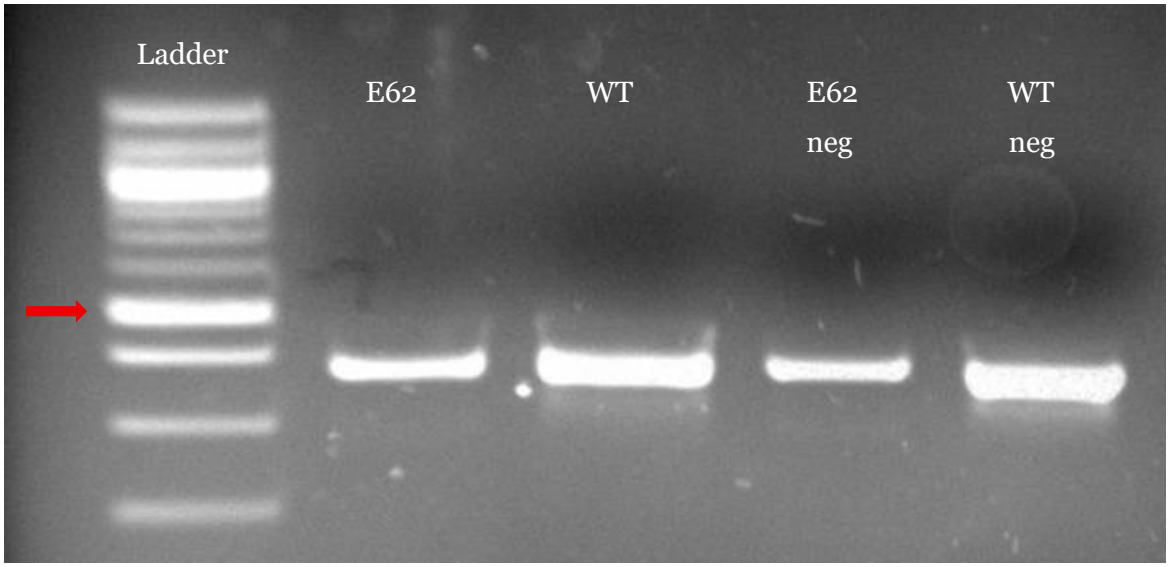

Figure 12: FastDigest Alw44I digestion of KFH E62 and wild-type (WT) samples, including undigested negative (neg) controls. The red arrow marks 500 bp. Ladder: Quick-Load® 100 bp DNA Ladder (New England Biolabs).

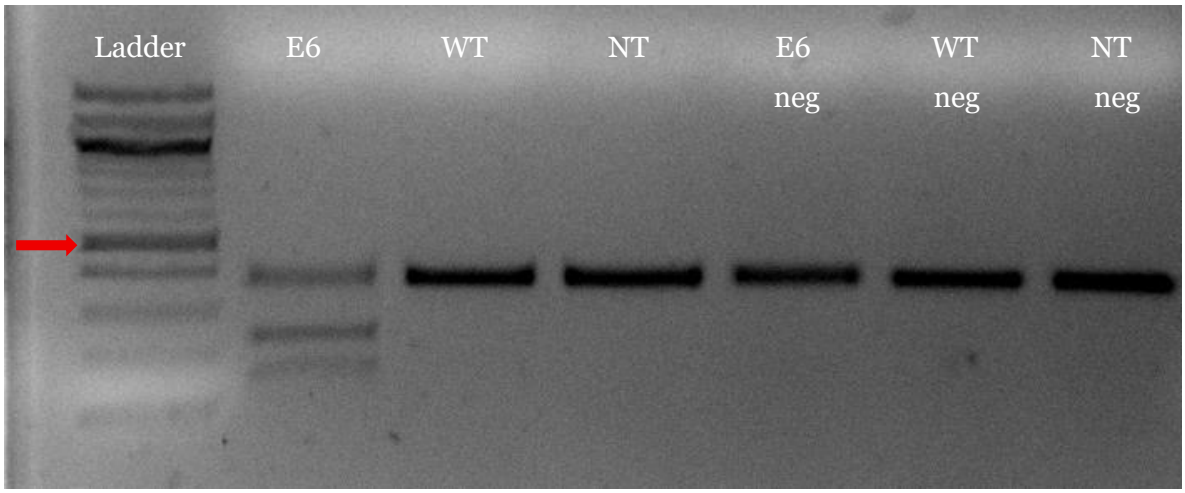

Figure 13: FastDigest Alw44I digestion of KFH E6, wild-type (WT), and non-targeting (NT) samples, including undigested negative controls. The red arrow marks 500 bp. Ladder: Quick-Load® 100 bp DNA Ladder (New England Biolabs).

For the CAPS clones analyzed by restriction digestion, all three samples showed several bands following the FastDigest TaqI digestion (Figures 14 and 15). The presence of multiple bands was consistent with the expected wild-type digestion pattern. Successful editing should have shown one single band. All undigested negative controls showed a single band at approximately 244 bp, corresponding to the expected PCR product size with CAPS primers. To confirm the restriction digestion results and determine whether the intended edit had been successfully introduced, samples C8 and D3 were selected for Sanger sequencing.

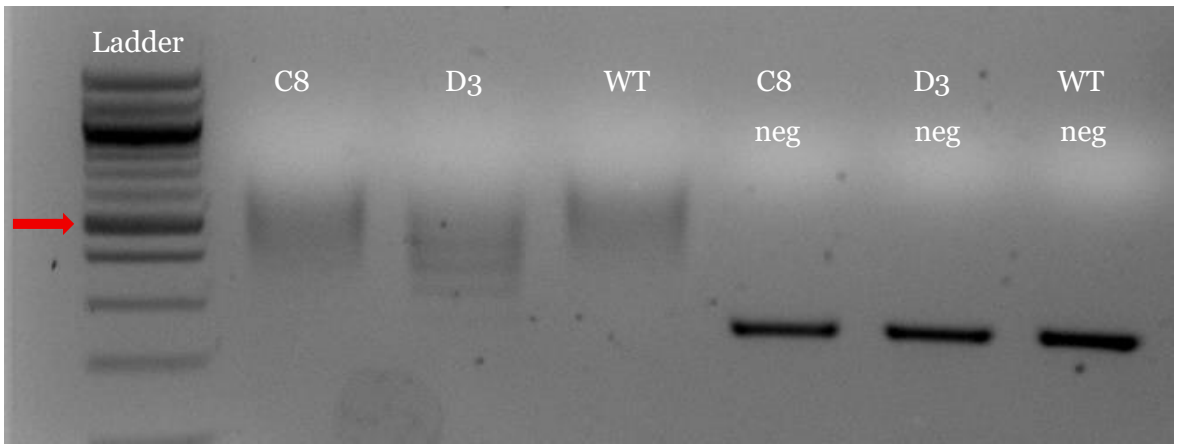

Figure 14: FastDigest TaqI digestion of CAPS C8, D3, and wild-type (WT) samples, including undigested negative (neg) controls. The red arrow marks 500 bp. Ladder: Quick-Load® 100 bp DNA Ladder (New England Biolabs).

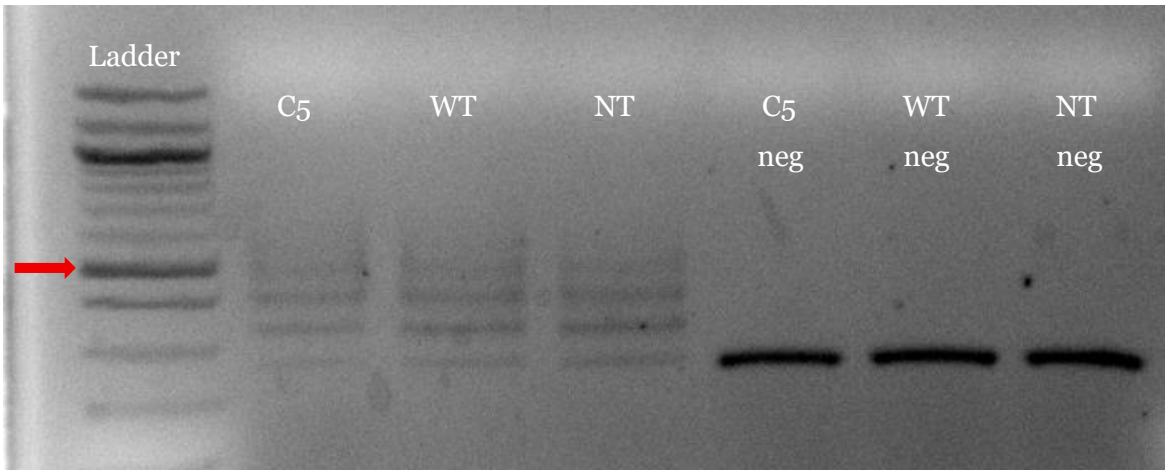

Figure 15: FastDigest TaqI digestion of CAPS C5, wild-type (WT), and non-targeting (NT) samples, including undigested negative (neg) controls. The red arrow marks 500 bp. Ladder: Quick-Load® 100 bp DNA Ladder (New England Biolabs).

4.4 Validation of the edit with Sanger sequencing

Sanger sequencing was performed to validate the restriction digestion results and to confirm the presence of the intended *NLRP3* variants in selected KFH and CAPS clones. Wild-type (WT) samples amplified with both KFH and CAPS primers were included as reference controls, and sequence data were analyzed against the human reference genome assembly GRCh38.

Sequencing of the KFH E62 sample was aligned with the wild-type reference (Figure 16) sequence at the target site (Figure 17). Both forward and reverse reads contained the wild-type nucleotide G at position c.61, and the intended c.61G>C substitution was not detected. The WT control also matched the reference sequence.

Sequencing of the KFH E6 sample produced less clear results (Figure 18). While most reads were consistent with the reference sequence, ambiguous nucleotide calls (M and S) were observed at the target position in both forward and reverse reads.

CAPS clones D3 and C8 were also analyzed by Sanger sequencing (Figure 20). At the target site, both clones showed the wild-type nucleotide C instead of the expected edited nucleotide T. The reverse reads of both samples were of low quality in the region surrounding the target site, resulting in missing nucleotide calls. However, all interpretable sequencing reads were consistent with the wild-type sequence (Figure 19).

Overall, Sanger sequencing did not confirm the presence of the intended KFH-associated c.61G>C variant or the CAPS-associated c.778_780delinsTGG variant in any of the analyzed clones. The sequencing results were therefore consistent with the restriction digestion analysis and indicated that successful genome editing could not be verified in the selected cell populations.

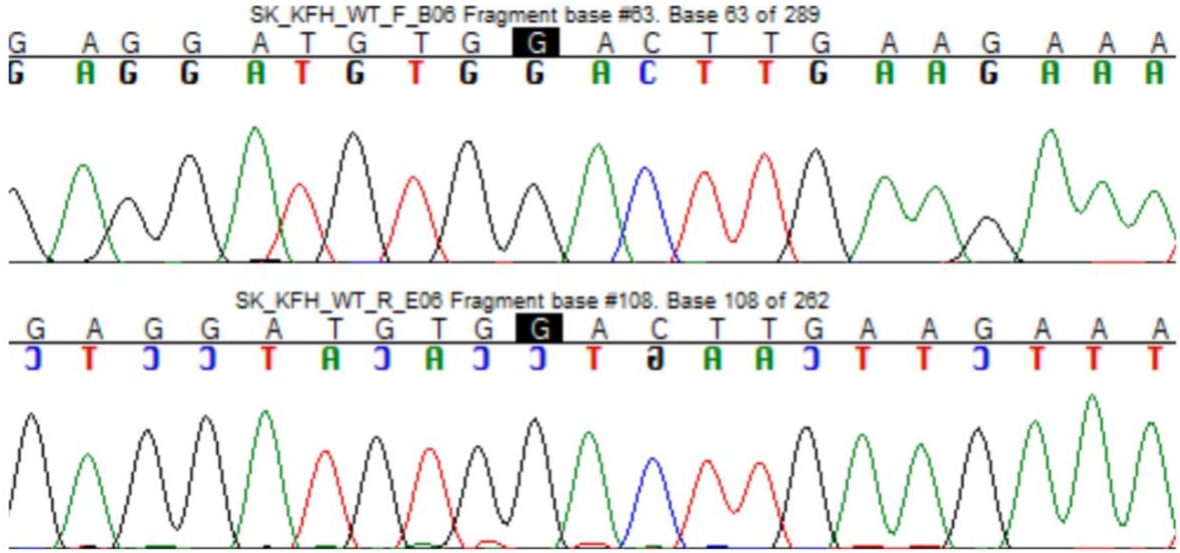

Figure 16: Sanger sequencing chromatogram for wild-type (WT) sample with KFH primers. Forward strand is upper and reverse strand lower. Highlighted (in black) G indicates the targeted nucleotide.

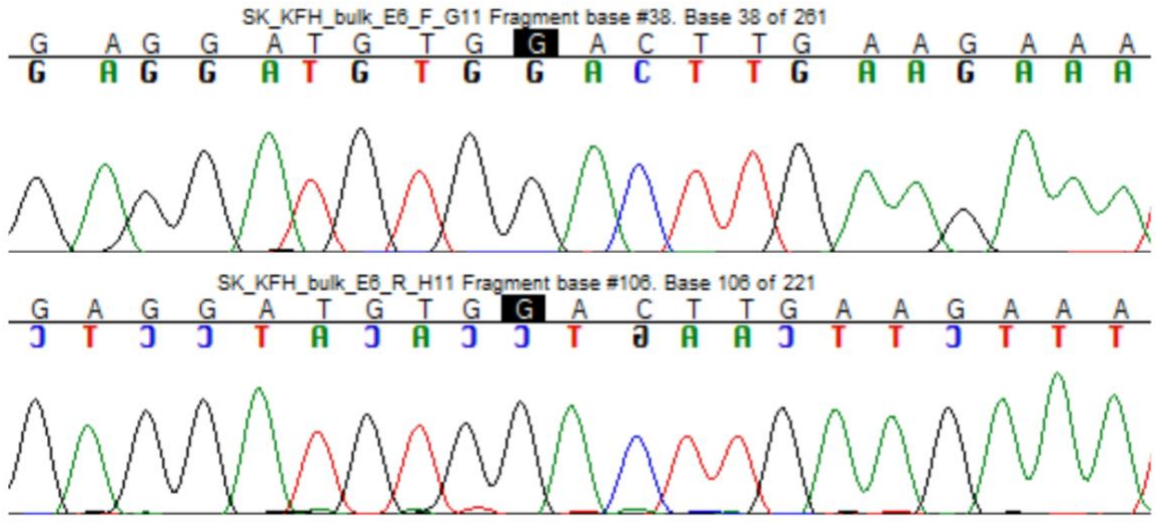

Figure 17: Sanger sequencing chromatogram for KFH E62 forward (upper) and reverse (lower) strands. Highlighted (in black) G indicates the targeted nucleotide.

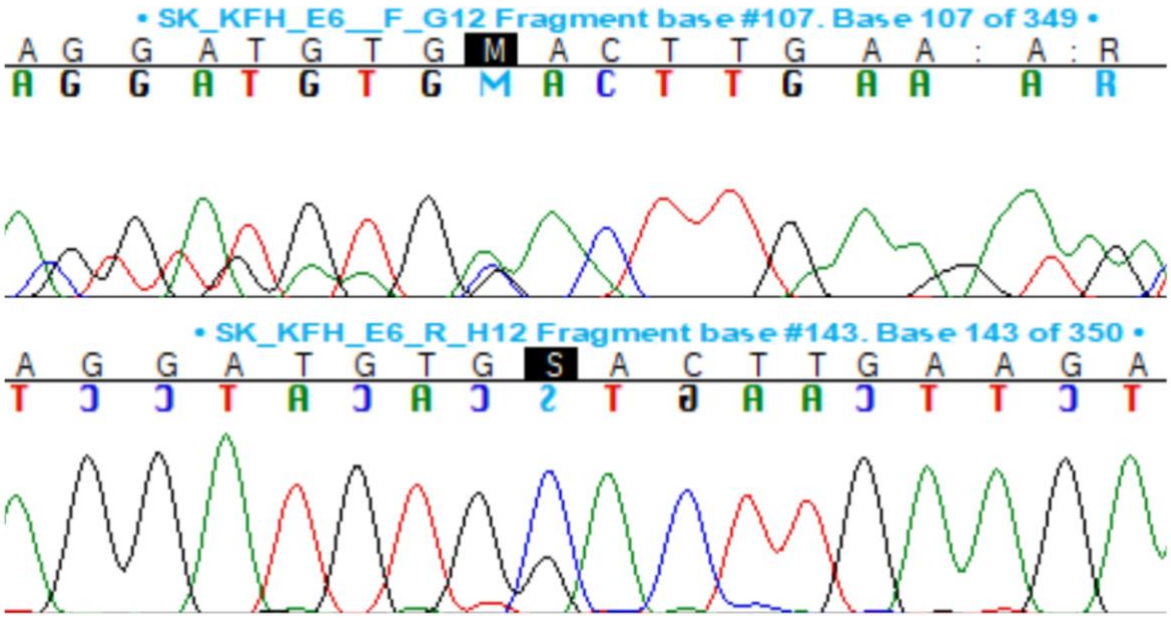

Figure 18: Sanger sequencing chromatogram for KFH E6 forward (upper) and reverse (lower) strands. Highlighted (in black) M and S indicate the targeted nucleotide.

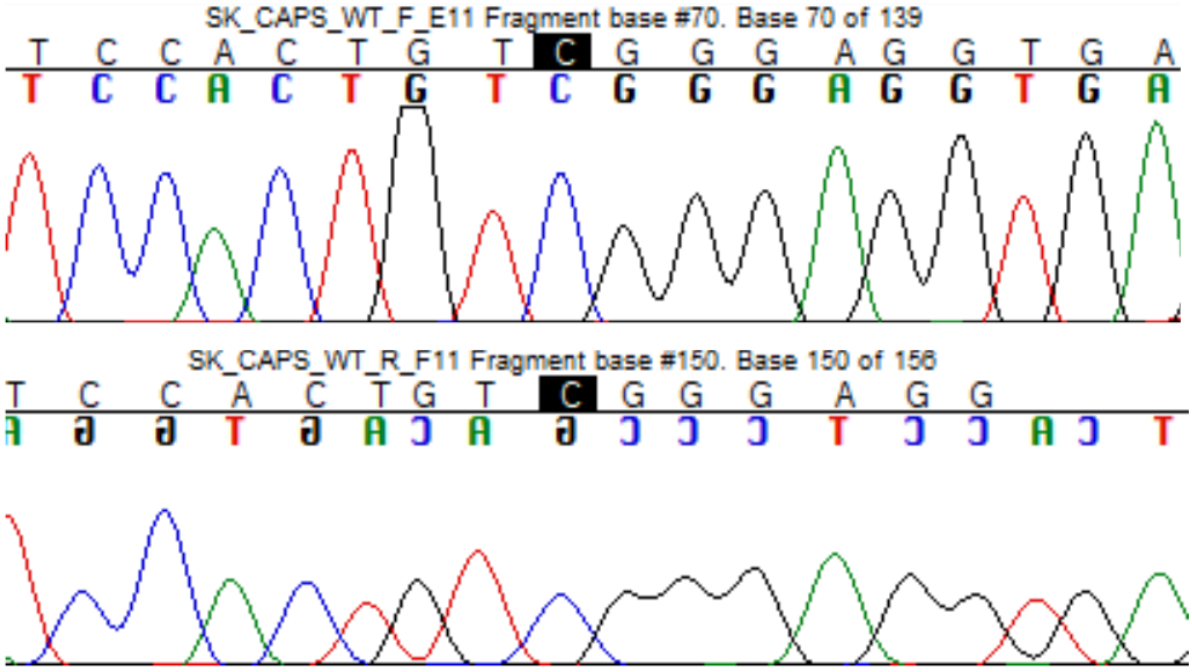

Figure 19: Sanger sequencing chromatogram for wild-type (WT) sample with CAPS primers. Forward strand is upper and reverse strand lower. Highlighted (in black) C indicates the targeted nucleotide.

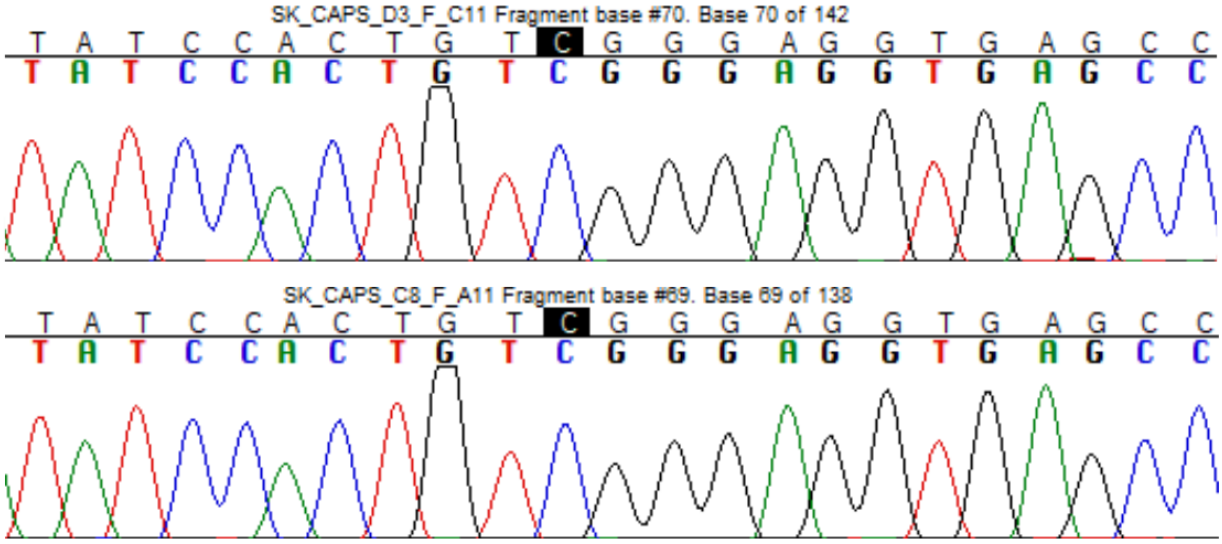

Figure 20: Sanger sequencing chromatogram for CAPS D3 (upper) and C8 (lower) forward strands. Highlighted (in black) C indicates the targeted nucleotide.

5 Discussion

The molecular mechanisms underlying keratitis fugax hereditaria (KFH) remain incompletely understood, partly because of the lack of suitable cellular models to investigate the effects of the disease-associated *NLRP3* c.61G>C, p.(Asp21His) variant. To address this limitation, this thesis project aimed to establish an *in vitro* KFH model by introducing the variant into THP-1 monocytic cells using CRISPR-Cas9 gene editing. While the intended variant was not confirmed in the clones examined, the study established a workflow for CRISPR-Cas9-mediated editing and provided valuable insights into the technical challenges of precise genome editing in THP-1 cells. These results offer a foundation for future optimization and development of a disease model for KFH.

5.1 Evaluation of CRISPR-Cas9 delivery strategy

One important outcome of this study was the successful delivery of CRISPR-Cas9 RNP complexes into THP-1 cells. FACS results showed a high proportion of ATTO™550-positive cells after electroporation, indicating efficient uptake of the CRISPR/Cas9 components. This suggests that delivery of the editing components was not a major limiting factor in this study. Efficient delivery is an important step in gene editing (Kim et al., 2014), and the high proportion of ATTO™550-positive cells indicates that electroporation could be a suitable method for introducing CRISPR-Cas9 components into THP-1 cells. Overall, the FACS results demonstrated successful transfection of the target cell populations and supported their use in downstream single-cell sorting. However, the results also demonstrate that successful delivery of CRISPR-Cas9 components does not necessarily result in successful gene editing. This is particularly relevant when precise nucleotide changes are introduced using HDR.

5.2 Factors potentially limiting the gene editing

Despite the efficient delivery of the CRISPR-Cas9 components, molecular analyses did not confirm successful introduction of either the KFH-associated variant or the CAPS-associated positive-control variant. Restriction digestion and Sanger sequencing consistently showed that the analyzed clones lacked the desired

nucleotide changes. One of the two KFH clones selected for restriction digestion and Sanger sequencing displayed an unexpected digestion pattern with three bands and produced ambiguous Sanger sequencing reads. According to the IUPAC nucleotide ambiguity code (Johnson, 2010), M indicates the presence of either adenine (A) or cytosine (C), whereas S indicates the presence of either guanine (G) or cytosine (C). These ambiguous signals suggest mixed base calling at the analyzed position and prevented reliable determination of the nucleotide sequence. Because the sequencing data did not unambiguously show the c.61G>C substitution, the clone could not be confirmed as successfully edited. Furthermore, the clone exhibited unusual growth characteristics and morphology compared with other expanding clones, including slower growth, altered cell size, and irregular clumping. Together, these observations may indicate a genomic alteration at the intended target site or elsewhere in the genome. However, technical artifacts, sample contamination, cellular debris, or the presence of a mixed cell population cannot be ruled out. Further analysis would be required to determine the origin of this result. The results from both restriction digestion and Sanger sequencing aligned, supporting the use of restriction digestion as an initial screening method before sequencing. This approach could reduce the amount of sequencing required when screening large numbers of clones.

Several factors may have contributed to the lack of successful editing. HDR is generally less efficient in human cells than NHEJ (X. He et al., 2016). HDR efficiency can be affected by several factors, including the cell cycle stage, donor template design, gRNA efficiency, and the cut-to-mutation distance (Paquet et al., 2016). Even when Cas9 successfully cuts the target DNA, the break may be repaired through NHEJ instead of HDR (Yang et al., 2020). This can result in a low frequency of precise nucleotide substitutions (Paquet et al., 2016). Therefore, editing events may have occurred at a frequency below the detection limit of the screening methods used in this study, or HDR-mediated repair may have occurred only in a very small number of cells.

Although the gRNAs were selected based on predicted specificity and on-target scores, computational predictions cannot completely exclude off-target cleavage. Off-target DSBs could potentially impair cell fitness, alter growth characteristics, cause unintended edits, or contribute to clone loss during expansion (Tycko et al., 2019; Özden & Minary, 2024). This possibility may be particularly relevant for the clone, which displayed an atypical restriction digestion pattern and ambiguous sequencing chromatograms. While these findings do not provide direct evidence of off-target

editing, they suggest that unintended genomic alterations cannot be ruled out without additional analyses. Notably, the KFH gRNA had a predicted on-target score of 32 and an off-target score of 0, indicating less favorable predicted editing characteristics than the CAPS guide (on-target 67; off-target 80). Although these computational scores do not demonstrate actual off-target editing, they suggest that unintended cleavage events may have occurred and could potentially explain the abnormal phenotype observed in the KFH clone. For both variants, however, these were the most suitable gRNA designs available in the IDT designing tool based on the criteria used in this study.

One possible explanation is that cells introduced with the CAPS variant were less likely to have a successful edit because the edited locus may have remained exposed to repeated Cas9 cleavage. CRISPR/Cas9 can repeatedly re-cut edited loci until NHEJ-mediated modification prevents further targeting, and this tendency for re-editing is a known source of corrupted or lost HDR outcomes (Paquet et al., 2016). In this study, no silent mutations were introduced into the donor template to prevent Cas9 recognition following HDR-mediated repair. This aspect should be carefully considered during experimental design. Silent mutations, preferably placed in the PAM, minimize undesirable re-editing during Cas9 cleavage (Medley et al., 2022; Schubert et al., 2021). For the CAPS c.778_780delinsTGG variant, this may have been particularly important, because the desired sequence included a TGG motif corresponding to the NGG PAM sequence that Cas9 requires for recognition and cleavage. Thus, it is possible that correctly edited alleles were generated but subsequently re-cut by Cas9, decreasing the overall efficiency of recovering successfully edited clones. In comparison, the KFH c.61G>C variant altered the target sequence in a way that was less dependent on having silent mutations added to the sequence.

5.3 Survival of sorted cells

In addition to the challenges related to gene editing, this study also revealed difficulties in single-cell cloning of THP-1 cells. After single-cell sorting, only a relatively small proportion of cells expanded into viable colonies suitable for further analysis. THP-1 cells may benefit from cell-to-cell interactions and factors released by nearby cells, which can make single-cell expansion more difficult. The low number of surviving

clones also reduced the likelihood of identifying successfully edited cells, especially when the expected editing frequency was low.

The limited clone recovery may reflect inherent characteristics of the THP-1 model. Although THP-1 cells are widely used in inflammasome research, THP-1 cells do not fully reproduce the heterogeneity, tissue-specific imprinting, or physiological maturation of primary human monocytes and macrophages. Differences have been reported in basal receptor expression, cytokine production, and responsiveness to inflammatory stimuli, particularly when THP-1 cells are compared directly with PBMCs (Chanput et al., 2014). The phenotype of THP-1 cells can also vary according to culture conditions and experimental handling, making the precise cellular state an important consideration when interpreting results (Attar et al., 2026).

Despite these limitations, THP-1 cells remain a valuable model for investigating innate immune mechanisms under controlled experimental conditions. Their reproducibility and experimental accessibility allow researchers to examine innate immune mechanisms under controlled conditions, compare responses across experiments, and evaluate molecular or pharmacological interventions. A review from 2014 (Chanput et al., 2014) further describes the use of THP-1 cells in studies of immune modulation, cell–cell interactions, and engineered reporter systems, while emphasizing that findings obtained with THP-1 cells should ultimately be validated in primary human cells or complementary experimental models.

The difficulties observed during clonal expansion highlight the need to further optimize the culture conditions used after single-cell sorting. Several approaches could be tested in future studies, such as the use of conditioned medium, growth-promoting supplements, or different cell densities during the recovery period. The effect of β-mercaptoethanol could also be investigated more but there isn’t yet any evidence on that matter. Improving the survival of single cells would increase the overall efficiency of the workflow and improve the chances of obtaining correctly edited clones.

Differences in growth after sorting were also observed between the KFH-targeted and CAPS-targeted populations. Although neither variant was confirmed, the CAPS-targeted cells appeared to form proliferating clones somewhat more easily than the KFH-targeted cells. Since the intended mutations were not verified, these observations cannot be directly linked to the different target variants. However, the results highlight the importance of monitoring cell growth and viability throughout the editing and cloning process. Future studies could include more systematic

measurements of clone growth, viability, and proliferation to better identify factors affecting clone recovery.

5.4 Future aspects

Future studies should focus on improving both editing efficiency and clone recovery. One practical approach would be to increase the number of single cells sorted and to establish a larger number of independent clones for screening. Since HDR-mediated editing events can be rare, screening a larger number of clones would increase the chance of identifying correctly edited cells. At the same time, optimization of the donor template, nucleofection conditions, and HDR donor oligo design could further improve the editing efficiency. HDR could also be enhanced by suppressing the competing NHEJ pathway or by knocking down key NHEJ proteins (Liu et al., 2019).

Newer genome-editing technologies may also provide alternative approaches for generating a KFH disease model. Base editing and prime editing can introduce precise nucleotide changes without requiring DSBs (Anzalone et al., 2019; Komor et al., 2016). By bypassing DSBs, these methods avoid the random insertions, deletions, and chromosomal rearrangements that are typical in HDR-based editing (Komor et al., 2016). Prime editing is particularly versatile, capable of mediating all twelve possible base-to-base conversions, including transversions like the G to C change required for the *NLRP3* c.61G>C variant (Anzalone et al., 2019; Chen & Liu, 2022). These methods may therefore overcome some of the limitations associated with HDR-based editing. Future studies could investigate whether base editing or prime editing provides a more efficient approach for generating the desired variant in THP-1 cells.

Once a validated KFH cell model has been established, it could be used to investigate the cellular and molecular mechanisms underlying the disease. Functional studies could examine NLRP3 inflammasome activation, secretion of IL-1β and IL-18, pyroptotic cell death, and other inflammatory signaling pathways associated with the mutant *NLRP3*. Comparison with established models of CAPS could also provide information about how different *NLRP3* variants affect inflammasome function and contribute to different disease phenotypes. These studies could help identify disease-specific mechanisms that may be relevant for future therapeutic approaches.

5.5 Conclusions

In conclusion, this thesis established and evaluated a CRISPR/Cas9 gene editing workflow to generate an *in vitro* cell model of keratitis fugax hereditaria. Although the intended variant was not confirmed in the clones examined, the study identified important technical challenges related to HDR-mediated editing and single-cell expansion. The findings show that both the gene editing strategy and cell-culture conditions need careful optimization when developing disease models using suspension cell lines. Despite the lack of a validated KFH model, the workflow established in this study provides a useful basis for future work. Further optimization of gRNA design, donor templates, and clone recovery, along with the use of newer gene editing technologies, may improve the chances of successfully generating a KFH disease model. Such a model could provide a valuable platform for further investigation of KFH pathogenesis and the development of targeted therapeutic strategies.

6 Acknowledgments

I would like to thank my supervisors, Docent MD Joni Turunen and PhD researcher Sabita Kawan, for their guidance, support, and valuable feedback throughout this thesis project. Their expertise has been invaluable at every stage of the work.

I am especially grateful to Sabita for her guidance in the laboratory and for always being willing to share her knowledge and advice. I would also like to thank all members of the Eye Genetics Group for warmly welcoming me into the group and for creating a supportive and inspiring research environment.

I also want to acknowledge the Biomedicum Flow Cytometry Unit and Imaging Unit for their services, as well as the Institute for Molecular Medicine Finland (FIMM) Genomics Unit, supported by HiLIFE and Biocenter Finland, for providing Sanger sequencing services.

Finally, I thank my family and friends for their encouragement, patience, and support throughout my studies and during the completion of this thesis. Special thanks to Senja and Milla for keeping me company during coffee breaks and for helping maintain a healthy balance between science and everything else.

References

Alejandre, N., Ruiz-Palacios, A., García-Aparicio, A. M., Blanco-Kelly, F., Bermúdez, S., Fernández-Sanz, G.,…Sánchez-Pernaute, O. (2014). Description of a new family with cryopyrin-associated periodic syndrome: risk of visual loss in patients bearing the R260W mutation. *Rheumatology*, *53*(6), 1095-1099. https://doi.org/10.1093/rheumatology/ket486

Alenezi, H., Parnell, G., Schibeci, S., Ozkan, J., Willcox, M., White, A., & Carnt, N. (2024). Ocular surface immune transcriptome and tear cytokines in corneal infection patients. *Frontiers in Cellular and Infection Microbiology*, *14*. https://doi.org/10.3389/fcimb.2024.1346821

Almeida-Da-Silva, C., Savio, L., Coutinho-Silva, R., & Ojcius, D. (2023). The role of NOD-like receptors in innate immunity. *Frontiers in Immunology*, *14*. https://doi.org/10.3389/fimmu.2023.1122586

Amarante-Mendes, G., Adjemian, S., Branco, L., Zanetti, L., Weinlich, R., & Bortoluci, K. (2018). Pattern Recognition Receptors and the Host Cell Death Molecular Machinery. *Frontiers in Immunology*, *9*. https://doi.org/10.3389/fimmu.2018.02379

Anzalone, A., Randolph, P., Davis, J., Sousa, A., Koblan, L., Levy, J.,…Liu, D. (2019). Search-and-replace genome editing without double-strand breaks or donor DNA. *Nature*, *576*, 149-157. https://doi.org/10.1038/s41586-019-1711-4

Attar, N., Rajabli, N., Chary, A., Stoffels, C. B. A., Serchi, T., & Weber, P. (2026). Phenotypic and functional characterization of THP-1-derived macrophages: impact of serum and serum-free differentiation conditions on surface marker expression and immune function [Original Research]. *Frontiers in Toxicology*, *Volume 8 - 2026*. https://doi.org/10.3389/ftox.2026.1843205

Auwerx, J. (1991). The human leukemia cell line, THP-1: a multifacetted model for the study of monocyte-macrophage differentiation. *Experientia*, *47*(1), 22-31. https://doi.org/10.1007/bf02041244

Barton, G. M. (2008). A calculated response: control of inflammation by the innate immune system. *The Journal of Clinical Investigation*, *118*(2), 413-420. https://doi.org/10.1172/JCI34431

Beuerman, R. W., & Pedroza, L. (1996). Ultrastructure of the human cornea. *Microsc Res Tech*, *33*(4), 320-335. https://doi.org/10.1002/(sici)1097-0029(19960301)33:4<320::Aid-jemt3>3.0.Co;2-t

Booshehri, L. M., & Hoffman, H. M. (2019). CAPS and NLRP3. *Journal of Clinical Immunology*, *39*(3), 277-286. https://doi.org/10.1007/s10875-019-00638-z

Bosshart, H., & Heinzelmann, M. (2016). THP-1 cells as a model for human monocytes. *Annals of Translational Medicine*, *4*(21), 438.

Broz, P., & Dixit, V. M. (2016). Inflammasomes: mechanism of assembly, regulation and signalling. *Nature Reviews Immunology*, *16*(7), 407-420. https://doi.org/10.1038/nri.2016.58

Chan, A., & Schroder, K. (2019). Inflammasome signaling and regulation of interleukin-1 family cytokines. *The Journal of Experimental Medicine*, *217*. https://doi.org/10.1084/jem.20190314

Chanput, W., Mes, J. J., & Wichers, H. J. (2014). THP-1 cell line: An in vitro cell model for immune modulation approach. *International Immunopharmacology*, *23*(1), 37-45. https://doi.org/https://doi.org/10.1016/j.intimp.2014.08.002

Chen, L., Deng, H., Cui, H., Fang, J., Zuo, Z., Deng, J.,…Zhao, L. (2018). Inflammatory responses and inflammation-associated diseases in organs. *Oncotarget*, *9*(6), 7204-7218. https://doi.org/10.18632/oncotarget.23208

Chen, P., & Liu, D. (2022). Prime editing for precise and highly versatile genome manipulation. *Nature reviews. Genetics*, *24*, 161-177. https://doi.org/10.1038/s41576-022-00541-1

Chen, Y., Ye, X., Escames, G., Lei, W., Zhang, X., Li, M.,…Yang, Y. (2023). The NLRP3 inflammasome: contributions to inflammation-related diseases. *Cellular & Molecular Biology Letters*, *28*(1), 51. https://doi.org/10.1186/s11658-023-00462-9

Coll, R. C., Schroder, K., & Pelegrín, P. (2022). NLRP3 and pyroptosis blockers for treating inflammatory diseases. *Trends in Pharmacological Sciences*, *43*(8), 653-668. https://doi.org/https://doi.org/10.1016/j.tips.2022.04.003

Daigneault, M., Preston, J. A., Marriott, H. M., Whyte, M. K., & Dockrell, D. H. (2010). The identification of markers of macrophage differentiation in PMA-stimulated THP-1 cells and monocyte-derived macrophages. *PLoS One*, *5*(1), e8668. https://doi.org/10.1371/journal.pone.0008668

DelMonte, D. W., & Kim, T. (2011). Anatomy and physiology of the cornea. *Journal of Cataract & Refractive Surgery*, *37*(3), 588-598. https://doi.org/10.1016/j.jcrs.2010.12.037

Doudna, J. A., & Charpentier, E. (2014). The new frontier of genome engineering with CRISPR-Cas9. *Science*, *346*(6213), 1258096. https://doi.org/doi:10.1126/science.1258096

Downie, L. E., Zhang, X., Wu, M., Karunaratne, S., Loi, J. K., Senthil, K.,…Chinnery, H. R. (2023). Redefining the human corneal immune compartment using dynamic intravital imaging. *Proceedings of the National Academy of Sciences*, *120*(31), e2217795120. https://doi.org/doi:10.1073/pnas.2217795120

Duan, T., Du, Y., Xing, C., Wang, H., & Wang, R. F. (2022). Toll-Like Receptor Signaling and Its Role in Cell-Mediated Immunity. *Frontiers in Immunology*, *13*. https://doi.org/10.3389/fimmu.2022.812774

Eghrari, A., Riazuddin, S., & Gottsch, J. (2015). Overview of the Cornea: Structure, Function, and Development. *Progress in molecular biology and translational science*, *134*, 7-23. https://doi.org/10.1016/bs.pmbts.2015.04.001

Feng, S., Wierzbowski, M., Hrovat-Schaale, K., Dumortier, A., Zhang, Y., Zyulina, M.,…Masters, S. (2025). Mechanisms of NLRP3 activation and inhibition elucidated by functional analysis of disease-associated variants. *Nature Immunology*, *26*, 511-523. https://doi.org/10.1038/s41590-025-02088-9

Ge, J., Li, X., Xia, Y., Chen, Z., Xie, C., Zhao, Y.,…Tong, J. (2024). Recent Advances in NLRP3 Inflammasome in Corneal Diseases: Preclinical Insights and Therapeutic Implications. *The ocular surface*. https://doi.org/10.1016/j.jtos.2024.09.007

Guo, H., Callaway, J. B., & Ting, J. P. Y. (2015). Inflammasomes: mechanism of action, role in disease, and therapeutics. *Nature Medicine*, *21*(7), 677-687. https://doi.org/10.1038/nm.3893

He, W.-t., Wan, H., Hu, L., Chen, P., Wang, X., Huang, Z.,…Han, J. (2015). Gasdermin D is an executor of pyroptosis and required for interleukin-1β secretion. *Cell Research*, *25*(12), 1285-1298. https://doi.org/10.1038/cr.2015.139

He, X., Tan, C., Wang, F., Wang, Y., Zhou, R., Cui, D.,…Feng, B. (2016). Knock-in of large reporter genes in human cells via CRISPR/Cas9-induced homology-dependent and independent DNA repair. *Nucleic Acids Res*, *44*(9), e85. https://doi.org/10.1093/nar/gkw064

He, Y., Zeng, M., Yang, D., Motro, B., & Núñez, G. (2016). Nek7 is an essential mediator of NLRP3 activation downstream of potassium efflux. *Nature*, *530*, 354-357. https://doi.org/10.1038/nature16959

Herzenberg, L. A., Parks, D., Sahaf, B., Perez, O., Roederer, M., & Herzenberg, L. A. (2002). The history and future of the fluorescence activated cell sorter and flow cytometry: a view from Stanford. *Clin Chem*, *48*(10), 1819-1827.

Hille, F., & Charpentier, E. (2016). CRISPR-Cas: biology, mechanisms and relevance. *Philos Trans R Soc Lond B Biol Sci*, *371*(1707). https://doi.org/10.1098/rstb.2015.0496

Immonen, A. T., Kawan, S., Backlund, M. P., Saaren-SeppÄLÄ, H., KivelÄ, T. T., & Turunen, J. A. (2025). Errors and Delays in Diagnosing Keratitis Fugax Hereditaria. *American Journal of Ophthalmology*, *274*, 122-130. https://doi.org/https://doi.org/10.1016/j.ajo.2025.03.004

Jiang, F., & Doudna, J. A. (2017). CRISPR–Cas9 Structures and Mechanisms. *Annual Review of Biophysics*, *46*(Volume 46, 2017), 505-529. https://doi.org/https://doi.org/10.1146/annurev-biophys-062215-010822

Jinek, M., Chylinski, K., Fonfara, I., Hauer, M., Doudna, J. A., & Charpentier, E. (2012). A programmable dual-RNA-guided DNA endonuclease in adaptive bacterial immunity. *Science*, *337*(6096), 816-821. https://doi.org/10.1126/science.1225829

Johnson, A. D. (2010). An extended IUPAC nomenclature code for polymorphic nucleic acids. *Bioinformatics*, *26*(10), 1386-1389. https://doi.org/10.1093/bioinformatics/btq098

Kawan, S., Backlund, M. P., Immonen, A. T., Kivelä, T. T., & Turunen, J. A. (2024). Functional consequences of pathogenic variant c.61G>C in the inflammasome gene NLRP3 underlying keratitis fugax hereditaria. *Br J Ophthalmol*, *108*(2), 323-328. https://doi.org/10.1136/bjo-2022-321825

Kawasaki, T., & Kawai, T. (2014). Toll-Like Receptor Signaling Pathways. *Frontiers in Immunology*, *5*. https://doi.org/10.3389/fimmu.2014.00461

Kelley, N., Jeltema, D., Duan, Y., & He, Y. (2019). The NLRP3 Inflammasome: An Overview of Mechanisms of Activation and Regulation. *Int J Mol Sci*, *20*(13). https://doi.org/10.3390/ijms20133328

Kim, S., Kim, D., Cho, S. W., Kim, J., & Kim, J.-S. (2014). Highly efficient RNA-guided genome editing in human cells via delivery of purified Cas9 ribonucleoproteins. *Genome Research*, *24*(6), 1012-1019. https://doi.org/10.1101/gr.171322.113

Kivelä, T. (2022). Keratitis fugax hereditaria: hiding in plain sight in Sweden? *Acta Ophthalmologica*, *100*. https://doi.org/10.1111/aos.15064

Komor, A., Kim, Y., Packer, M., Zuris, J., & Liu, D. (2016). Programmable editing of a target base in genomic DNA without double-stranded DNA cleavage. *Nature*, *533*, 420-424. https://doi.org/10.1038/nature17946

Lander, Eric S. (2016). The Heroes of CRISPR. *Cell*, *164*(1), 18-28. https://doi.org/https://doi.org/10.1016/j.cell.2015.12.041

Latz, E., Xiao, T. S., & Stutz, A. (2013). Activation and regulation of the inflammasomes. *Nature Reviews Immunology*, *13*(6), 397-411. https://doi.org/10.1038/nri3452

Lechtenberg, B., Mace, P., & Riedl, S. (2014). Structural Mechanisms in NLR inflammasome signaling. *Current opinion in structural biology*, *0*, 17-25. https://doi.org/10.1016/j.sbi.2014.08.011

Liao, H., Wu, J., VanDusen, N., Li, Y., & Zheng, Y. (2024). CRISPR-Cas9-mediated homology-directed repair for precise gene editing. *Molecular Therapy. Nucleic Acids*, *35*. https://doi.org/10.1016/j.omtn.2024.102344

Liu, M., Rehman, S., Tang, X., Gu, K., Fan, Q., Chen, D., & Ma, W. (2019). Methodologies for Improving HDR Efficiency [Review]. *Frontiers in Genetics*, *Volume 9 - 2018*. https://doi.org/10.3389/fgene.2018.00691

Mandell, J., Vaccari, J., Sabater, A., & Galor, A. (2022). The inflammasome pathway: A key player in ocular surface and anterior segment diseases. *Survey of ophthalmology*, *68*, 280-289. https://doi.org/10.1016/j.survophthal.2022.06.003

Medley, J. C., Hebbar, S., Sydzyik, J. T., & Zinovyeva, A. Y. (2022). Single nucleotide substitutions effectively block Cas9 and allow for scarless genome editing in Caenorhabditis elegans. *Genetics*, *220*(1). https://doi.org/10.1093/genetics/iyab199

Medzhitov, R. (2007). Recognition of microorganisms and activation of the immune response. *Nature*, *449*(7164), 819-826. https://doi.org/10.1038/nature06246

Meek, K. M., & Knupp, C. (2015). Corneal structure and transparency. *Progress in Retinal and Eye Research*, *49*, 1-16. https://doi.org/https://doi.org/10.1016/j.preteyeres.2015.07.001

Meizlish, M. L., Franklin, R. A., Zhou, X., & Medzhitov, R. (2021). Tissue Homeostasis and Inflammation. *Annual Review of Immunology*, *39*(Volume 39, 2021), 557-581. https://doi.org/https://doi.org/10.1146/annurev-immunol-061020-053734

Molina-López, C., Hurtado-Navarro, L., García, C. J., Angosto-Bazarra, D., Vallejo, F., Tapia-Abellán, A.,…Pelegrin, P. (2024). Pathogenic NLRP3 mutants form constitutively active inflammasomes resulting in immune-metabolic limitation of

IL-1β production. *Nature Communications*, *15*(1), 1096. https://doi.org/10.1038/s41467-024-44990-0

Moltrasio, C., Romagnuolo, M., & Marzano, A. V. (2022). NLRP3 inflammasome and NLRP3-related autoinflammatory diseases: From cryopyrin function to targeted therapies [Review]. *Frontiers in Immunology*, *Volume 13 - 2022*. https://doi.org/10.3389/fimmu.2022.1007705

Mun, Y., Kim, J., Choi, Y.-J., & Lee, B.-H. (2025). cGAS–STING–NF-κB Axis Mediates Rotenone-Induced NLRP3 Inflammasome Activation Through Mitochondrial DNA Release. *Antioxidants*, *14*. https://doi.org/10.3390/antiox14111276

Newton, K., & Dixit, V. M. (2012). Signaling in innate immunity and inflammation. *Cold Spring Harb Perspect Biol*, *4*(3). https://doi.org/10.1101/cshperspect.a006049

Paquet, D., Kwart, D., Chen, A., Sproul, A., Jacob, S., Teo, S.,…Tessier-Lavigne, M. (2016). Efficient introduction of specific homozygous and heterozygous mutations using CRISPR/Cas9. *Nature*, *533*(7601), 125-129. https://doi.org/10.1038/nature17664

Pinaud, M., & Zamborlini, A. (2025). Electroporation-Based CRISPR-Cas9-Mediated Gene Knockout in THP-1 Cells and Single-Cell Clone Isolation. *J Vis Exp*(216). https://doi.org/10.3791/67469

Platnich, J., & Muruve, D. (2019). NOD-like receptors and inflammasomes: A review of their canonical and non-canonical signaling pathways. *Archives of biochemistry and biophysics*. https://doi.org/10.1016/j.abb.2019.02.008

Prieto-Nevárez, H., Tarango-García, A., Ollivier-Valenzuela, L. I., Álvarez-Cardona, A., & Lugo-Reyes, S. (2026). Immune Privilege of the Eye: A Delicate Balance Between Clarity and Chaos. *Ocular Immunology and Inflammation*, *34*, 1143-1155. https://doi.org/10.1080/09273948.2026.2677099

Próchnicki, T., Mangan, M., & Latz, E. (2016). Recent insights into the molecular mechanisms of the NLRP3 inflammasome activation. *F1000Research*, *5*. https://doi.org/10.12688/f1000research.8614.1

Ruusuvaara, P., & Setälä, K. (1987). Keratoendotheliitis fugax hereditaria. A clinical and specular microscopic study of a family with dominant inflammatory corneal disease. *Acta Ophthalmol (Copenh)*, *65*(2), 159-169. https://doi.org/10.1111/j.1755-3768.1987.tb06995.x

Schmid-Burgk, J., Chauhan, D., Schmidt, T., Ebert, T., Reinhardt, J., Endl, E., & Hornung, V. (2015). A Genome-wide CRISPR (Clustered Regularly Interspaced Short Palindromic Repeats) Screen Identifies NEK7 as an Essential Component of NLRP3 Inflammasome Activation*. *The Journal of Biological Chemistry*, *291*, 103-109. https://doi.org/10.1074/jbc.c115.700492

Schubert, M. S., Thommandru, B., Woodley, J., Turk, R., Yan, S., Kurgan, G.,…Rettig, G. R. (2021). Optimized design parameters for CRISPR Cas9 and Cas12a homology-directed repair. *Scientific Reports*, *11*(1), 19482. https://doi.org/10.1038/s41598-021-98965-y

Shimizu, H., Sakimoto, T., & Yamagami, S. (2019). Pro-inflammatory role of NLRP3 inflammasome in experimental sterile corneal inflammation. *Scientific Reports*, *9*. https://doi.org/10.1038/s41598-019-46116-9

Soares, C. L. R., Wilairatana, P., Silva, L. R., Moreira, P. S., Vilar Barbosa, N. M. M., da Silva, P. R.,…Felipe, C. F. B. (2023). Biochemical aspects of the inflammatory process: A narrative review. *Biomedicine & Pharmacotherapy*, *168*, 115764. https://doi.org/https://doi.org/10.1016/j.biopha.2023.115764

Soliman, A., & Barreda, D. (2022). Acute Inflammation in Tissue Healing. *International Journal of Molecular Sciences*, *24*. https://doi.org/10.3390/ijms24010641

Sridhar, M. S. (2018). Anatomy of cornea and ocular surface. *Indian J Ophthalmol*, *66*(2), 190-194. https://doi.org/10.4103/ijo.IJO_646_17

Sundaram, B., Tweedell, R., Kumar, S. P., & Kanneganti, T. (2024). The NLR family of innate immune and cell death sensors. *Immunity*, *57*, 674-699. https://doi.org/10.1016/j.immuni.2024.03.012

Swanson, K. V., Deng, M., & Ting, J. P. Y. (2019). The NLRP3 inflammasome: molecular activation and regulation to therapeutics. *Nature Reviews Immunology*, *19*(8), 477-489. https://doi.org/10.1038/s41577-019-0165-0

Sáez, A., Herrero-Fernández, B., Gómez-Bris, R., Sánchez-Martinez, H., & González-Granado, J. (2023). Pathophysiology of Inflammatory Bowel Disease: Innate Immune System. *International Journal of Molecular Sciences*, *24*. https://doi.org/10.3390/ijms24021526

Taylor, A. W., & Ng, T. F. (2018). Negative regulators that mediate ocular immune privilege. *Journal of Leukocyte Biology*, *103*(6), 1179-1187. https://doi.org/10.1002/jlb.3mir0817-337r

Tuft, S. J., & Coster, D. J. (1990). The corneal endothelium. *Eye*, *4*(3), 389-424. https://doi.org/10.1038/eye.1990.53

Turunen, J. A., Immonen, A. T., Järvinen, R.-S., Kawan, S., Repo, P., Korsbäck, A.,…Kivelä, T. T. (2020). In Vivo Corneal Confocal Microscopy and Histopathology of Keratitis Fugax Hereditaria From a Pathogenic Variant in NLRP3. *American Journal of Ophthalmology*, *213*, 217-225. https://doi.org/https://doi.org/10.1016/j.ajo.2020.02.002

Turunen, J. A., Wedenoja, J., Repo, P., Järvinen, R.-S., Jäntti, J. E., Mörtenhumer, S.,…Kivelä, T. T. (2018). Keratoendotheliitis Fugax Hereditaria: A Novel Cryopyrin-Associated Periodic Syndrome Caused by a Mutation in the Nucleotide-Binding Domain, Leucine-Rich Repeat Family, Pyrin Domain-Containing 3 (NLRP3) Gene. *American Journal of Ophthalmology*, *188*, 41-50. https://doi.org/https://doi.org/10.1016/j.ajo.2018.01.017

Tycko, J., Wainberg, M., Marinov, G., Ursu, O., Hess, G., Ego, B.,…Bassik, M. (2019). Mitigation of off-target toxicity in CRISPR-Cas9 screens for essential non-coding elements. *Nature Communications*, *10*. https://doi.org/10.1038/s41467-019-11955-7

Valle, O. (1966). Keratitis Fugax Hereditaria – a New Eye Syndrome. *Ophthalmologica*, *151*(5), 537-547. https://doi.org/10.1159/000304912

Wang, R., Lan, C., Benlagha, K., Camara, N. O. S., Miller, H., Kubo, M.,…Liu, C. (2024). The interaction of innate immune and adaptive immune system. *MedComm*, *5*(10), e714. https://doi.org/https://doi.org/10.1002/mco2.714

Wang, Y., Yin, C., Feng, L., Ma, L., Wei, Y., & Sheng, G. (2013). Sorting, identification and enrichment of side population cells in THP-1 acute monocytic leukemia cells. *Oncol Rep*, *29*(5), 1923-1931. https://doi.org/10.3892/or.2013.2316

Warrick, K., Vallez, C., Meibers, H., & Pasare, C. (2025). Bidirectional Communication Between the Innate and Adaptive Immune Systems. *Annual review of immunology*, *43*, 489-514. https://doi.org/10.1146/annurev-immunol-083122-040624

Wu, M., Fletcher, E. L., Chinnery, H. R., Downie, L. E., & Mueller, S. N. (2024). Redefining our vision: an updated guide to the ocular immune system. *Nature Reviews Immunology*, *24*(12), 896-911. https://doi.org/10.1038/s41577-024-01064-y

Xiao, L., Magupalli, V., & Wu, H. (2022). Cryo-EM structures of the active NLRP3 inflammasome disc. *Nature*, *613*, 595-600. https://doi.org/10.1038/s41586-022-05570-8

Xu, C. F., Lu, Z.-D., Luo, Y., Liu, Y., Cao, Z., Shen, S.,…Wang, J. (2018). Targeting of NLRP3 inflammasome with gene editing for the amelioration of inflammatory diseases. *Nature Communications*, *9*. https://doi.org/10.1038/s41467-018-06522-5

Xu, J., & Núñez, G. (2022). The NLRP3 inflammasome: activation and regulation. *Trends in biochemical sciences*. https://doi.org/10.1016/j.tibs.2022.10.002

Yang, H., Ren, S., Yu, S., Pan, H., Li, T., Ge, S.,…Xia, N. (2020). Methods Favoring Homology-Directed Repair Choice in Response to CRISPR/Cas9 Induced-Double Strand Breaks. *Int J Mol Sci*, *21*(18). https://doi.org/10.3390/ijms21186461

Yang, Y., Wang, H., Kouadir, M., Song, H., & Shi, F. (2019). Recent advances in the mechanisms of NLRP3 inflammasome activation and its inhibitors. *Cell Death & Disease*, *10*. https://doi.org/10.1038/s41419-019-1413-8

Yao, J., Sterling, K., Wang, Z., Zhang, Y., & Song, W. (2024). The role of inflammasomes in human diseases and their potential as therapeutic targets. *Signal Transduction and Targeted Therapy*, *9*(1), 10. https://doi.org/10.1038/s41392-023-01687-y

Yu, X., Matico, R., Miller, R., Chauhan, D., Van Schoubroeck, B., Grauwen, K.,…Sharma, S. (2024). Structural basis for the oligomerization-facilitated NLRP3 activation. *Nature Communications*, *15*. https://doi.org/10.1038/s41467-024-45396-8

Zhou, R., & Caspi, R. R. (2010). Ocular immune privilege. *F1000 Biol Rep*, *2*. https://doi.org/10.3410/b2-3

Zindel, J., & Kubes, P. (2020). DAMPs, PAMPs, and LAMPs in Immunity and Sterile Inflammation. *Annu Rev Pathol*, *15*, 493-518. https://doi.org/10.1146/annurev-pathmechdis-012419-032847

Zito, G., Buscetta, M., Cimino, M., Dino, P., Bucchieri, F., & Cipollina, C. (2020). Cellular Models and Assays to Study NLRP3 Inflammasome Biology. *International Journal of Molecular Sciences*, *21*(12), 4294.

Özden, F. C., & Minary, P. (2024). Learning to quantify uncertainty in off-target activity for CRISPR guide RNAs. *Nucleic Acids Research*, *52*. https://doi.org/10.1093/nar/gkae759

Use of AI

Artificial intelligence (AI) tools were used to support the writing process of this thesis. Microsoft 365 Copilot (GPT-5) and Consensus (Gemini 3.8 Flash) were employed to assist with finding relevant peer-reviewed studies, grammar correction, and improvements in clarity and readability. All outputs generated by these tools were carefully evaluated, revised, and integrated by the author. The author takes full responsibility for the content of the thesis, including its accuracy, interpretation, and originality.